Inorganic Chemistry

Article

pubs.acs.org/IC

Structural and Photophysical Properties of Visible- and Near-IR-Emitting Tris Lanthanide(III) Complexes Formed with the Enantiomers of *N,N′*-Bis(1-phenylethyl)-2,6-pyridinedicarboxamide

KimNgan T. Hua,[†] Jide Xu,[‡] Eliseo E. Quiroz,[†] Sabrina Lopez,[†] Andrew J. Ingram,[†] Victoria Anne Johnson,[†] Angela R. Tisch,[†] Ana de Bettencourt-Dias,[§] Daniel A. Straus,[†] and Gilles Muller*[,†]

[†]Department of Chemistry, San José State University, 1 Washington Square, San José, California 95192-0101, United States

[‡]Department of Chemistry, University of California, Berkeley, Berkeley, California 94720-1460, United States

[§]Department of Chemistry, University of Nevada, Reno, 1664 N. Virginia Street, Reno, Nevada 89557-0216, United States

Supporting Information

ABSTRACT: The enantiomers of *N,N′*-bis(1-phenylethyl)-2,6-pyridinedicarboxamide (**L**), namely, (*R,R*)-**1**, and (*S,S*)-**1**, react with Ln^{III} ions to give stable $[LnL_3]^{3+}$ complexes in an anhydrous acetonitrile solution and in the solid state, as evidenced by electrospray ionization mass spectrometry, NMR, luminescence titrations, and their X-ray crystal structures, respectively. All $[LnL_3]^{3+}$ complexes [Ln^{III} = Eu, Gd, Tb, and Yb; **L** = (*R,R*)-**1** and (*S,S*)-**1**] are isostructural and crystallize in the cubic space group *I*23. Although the small quantum yields of the Ln^{III}-centered luminescence clearly point to the poor efficiency of the luminescence sensitization by the ligand and the intersystem crossing and ligand-to-metal energy transfers, the ligand triplet-excited-state energy seems relatively well suited to sensitize many Ln^{III} ion's emission for instance, in the visible (Eu and Tb), near-IR (Nd and Yb), or both regions (Pr, Sm, Dy, Er, and Tm).

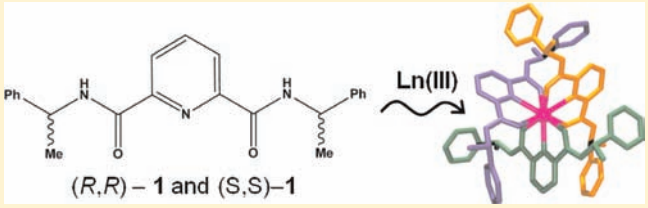

INTRODUCTION

Luminescent lanthanide(III) complex-based molecular probes are commonly employed for analytical and biomedical applications, where they are used as either diagnostic or therapeutic tools.[1−25] Although it is now commonplace to use them in fields like biochemistry, biology, medicine, and related biomedical disciplines, there is still a considerable surge of interest to develop luminescent lanthanide(III) compounds possessing chiral properties in addition to their interesting spectral features. These unusual spectral characteristics often consist of, e.g., long excited-state lifetimes, linelike emission bands that are easily recognizable and well separated from the broad fluorescence bands of the organic fluorophores, large Stokes' shift, sensitivity to the local environment, or time-resolved separation between lanthanide(III) luminescence and short-lived background fluorescence.

Dipicolinic acid (H_2dpa) and its derivatives are good candidates for the design of luminescent Ln^{III}-containing systems, as evidenced, for instance, by their use for chirality sensing.[26] Because these 9-coordinate lanthanide(III) compounds exist as racemic mixtures of complexes with Δ and Λ helicity in solution, one can use them toward the molecular recognition of chiral biological substrates. This is possible because of the observation of induced chirality in the latter upon outer-sphere coordination with a variety of optically active organic molecules such as tartrate substrates, amino acid, or sugar derivatives,[26−32] a phenomenon referred to as the "Pfeiffer effect".[33] Of special importance, it was shown that the chiral recognition of such biomolecular substrates can be modulated by the nature of the ligand interface of the racemic 9-coordinate lanthanide(III) complexes.[34] More recently, it was reported that the chiroptical spectroscopic circularly polarized luminescence (CPL) technique, the emission analogue to circular dichroism, has the potential for chiral recognition of optical isomers of a given amino acid.[26,27] This was possible because CPL is responsive to the nature and amount of the added chiral probes present in solution.

Because racemic lanthanide(III) complexes of ligands derived from H_2dpa are promising model systems for such studies and also because the modular nature of the backbone of H_2dpa allows for facile synthesis of derivatives with tunable photophysical and/or chiroptical properties,[35] we reported on the preparation of the optical isomers of *N,N′*-bis(1-phenylethyl)-2,6-pyridinedicarboxamide (**L**), namely, (*R,R*)-**1** and (*S,S*)-**1**, and their europium(III) complexes.[36] Of special importance, it was shown that these optical isomers of **L** formed stable 1:3 Eu^{III}:L complexes in an anhydrous acetonitrile solution and resulted in a CPL activity independent of the "age" of the solution (e.g., several months) and a lack of noticeable

Received: October 5, 2011
Published: December 7, 2011

   dx.doi.org/10.1021/ic202094p | *Inorg. Chem.* 2012, 51, 647−660

photochemical degradation under continuous UV excitation (e.g., 3 days). In addition to these interesting features, these Eu^{III}-containing compounds also possess chiroptical properties, as evidenced by their CPL activity, which may open new perspectives in the design of lanthanide(III) complexes acting as probes for chiral recognition because they may probe the chirality of biomolecules by the preferential interaction with one enantiomer. In particular, one can envisage that these Ln^{III}-based systems with more extended structures and also containing chiral substituents may lead to a diastereomeric resolution of the 9-coordinate lanthanide(III) complexes, as was already evidenced for the substituted pyridine-2,6-dicarboxamide ligand, $\mathbf{L}^4$, where a chiral group was grafted onto the para position of the pyridine group.[37] Although this ligand led to the formation of stable 1:3 complexes with log β_3 in the range of 19−20, there was only a very small excess of one diastereoisomer induced in solution by $\mathbf{L}^4$. This was corroborated by a weak CPL activity of the Ln^{III}-containing systems of interest. The calculated luminescence dissymmetry factor, g_{lum}, amounted to 0.02, a value much smaller than those reported for the 9-coordinate europium(III) complexes with the two optical isomers of **L**, (*R*,*R*)-**1** and (*S*,*S*)-**1** (−0.19 and +0.19, respectively), or other related systems.[36−40]

In this paper, we report on the interaction of the ligand **L** with trivalent Ln^{III} ions with an emphasis on the structural, thermodynamic, and photophysical properties of the resulting tris complexes, with Ln^{III} ions emitting in the visible and/or near-IR (NIR) regions. In addition to their potential use in chiral sensing applications, it is worth noting that such a study is of basic interest because the preliminary CPL results of the Eu^{III}-containing complexes led to the suggestion that the latter can be employed as reliable CPL calibration standards to perform accurate routine tests of CPL instrumentation at low cost.[36]

EXPERIMENTAL SECTION

General Procedures. Solvents and starting materials were purchased from Acros or Sigma-Aldrich and used without further purification unless otherwise stated. Acetonitrile, dichloromethane, and methanol were purified in the usual way. Lanthanide(III) trifluoromethanesulfonates, $Ln(Otf)_3$ (Ln^{III} = La and Eu), were prepared from lanthanum and europium oxides (Stanford Materials Corp., 99.995%) and dried according to published procedures. The Ln content of solutions was determined by complexometric titrations with a standardized solution of ethylenediaminetetraacetic acid in the presence of 0.1 M ammonium acetate and arsenazo III. Unless otherwise specified, all sample solutions for the photophysical studies were prepared and stored in a glovebox. The three isomers of **L**, (*R*,*R*)-, (*S*,*S*)-, and (*R*,*S*)-**1**, were synthesized as described previously.[36]

X-ray Experimental Section. Crystals suitable for X-ray analysis were mounted on a Kapton loop using Paratone N hydrocarbon oil and measured at low temperature using a Siemens SMART or APEX CCD[41] area detector with graphite-monochromated Mo Kα radiation (Tables 1 and S3 and S4 in the Supporting Information). Cell constants and orientation matrices were obtained from least-squares refinement. The resulting data were integrated by the program *SAINT*[42] and corrected for Lorentz and polarization effects. Data were also analyzed for agreement and possible absorption using *XPREP*.[43] An empirical absorption correction based on a comparison of the redundant and equivalent reflections was applied using *SADABS*.[44] Equivalent reflections were merged where appropriate, and no decay correction was applied. The structures were solved within the *WinGX*[45] package by direct methods using *SIR2004*[46] and expanded using a full-matrix least-squares techniques with *SHELXL-97*.[47] H atoms were positioned geometrically for all H atoms. The resulting drawings of molecules were produced with *ORTEP-3*.[48] In the lattice of these complexes, there are a few unresolved disordered methanol and water molecules, which were treated with the *SQUEEZE* routine included in *PLATON*;[49] the final refinement by this approach provided significantly better residuals.

Spectroscopic and Analytical Measurements. Optical rotation values were measured from 6.67×10^{-3} M solutions in anhydrous MeCN at 298 K with the help of a Rudolph Autopol III polarimeter

Scheme 1

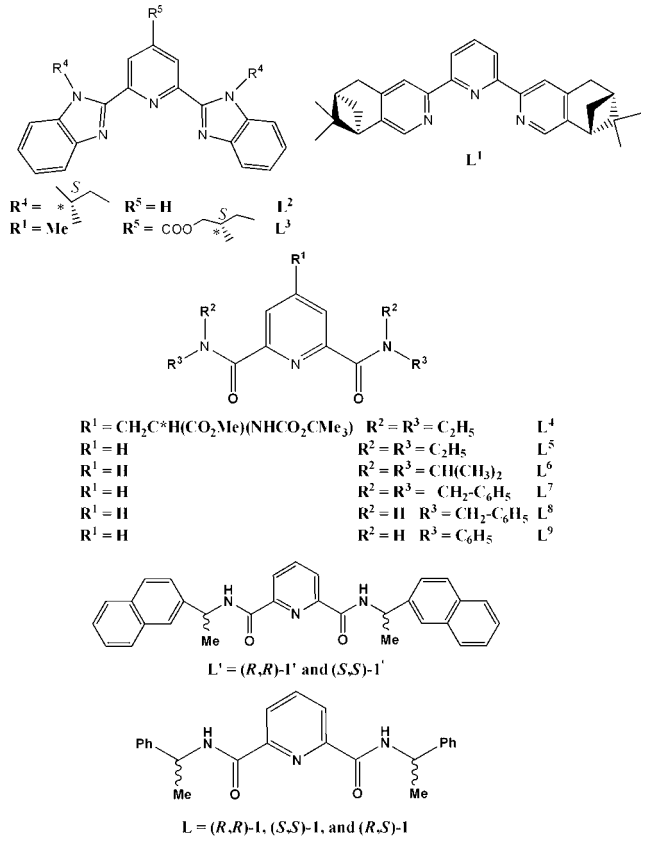

Table 1. Crystallographic Data for (*R*,*S*)-1 and $[LnL_3]^{3+}$ [Ln^{III} = Eu and Yb; L = (*R*,*R*)-1]

	(*R*,*S*)-**1**	$[EuL_3]^{3+}$	$[YbL_3]^{3+}$
empirical formula	$C_{23}H_{23}N_3O_2$	$C_{70.5}H_{75}Cl_3EuN_9O_{7.5}$	$C_{70.5}H_{75.75}Cl_3N_9O_{7.88}Yb$
fw	373.44	1426.70	1454.54
T (K)	149(2)	153(2)	147(2)
cryst syst	orthorhombic	cubic	cubic
space group	$P2_12_12_1$	$I23$	$I23$
a/Å	10.053(4)	25.946(2)	25.839
b/Å	10.513(4)	25.946(2)	25.839
c/Å	37.598(16)	25.946(2)	25.839
α/deg	90	90	90
β/deg	90	90	90
γ/deg	90	90	90
V/Å^3	3974	17 466	17 251.5
Z	8	8	8
abs coeff (mm^{-1})	0.081	0.857	1.225
D_c/(mg/m^3)	1.248	1.085	1.120
reflns collected	19 008	43 513	46 664
unique reflns	4213	5338	6812
R_{int}	0.0536	0.0335	0.0384
param	560	274	276
final R1 [$I > 2\sigma(I)$]	0.0350	0.0298	0.0292
wR2	0.0594	0.0834	0.0787

dx.doi.org/10.1021/ic202094p | *Inorg. Chem.* 2012, 51, 647−660

(sodium D line). ^{1}H and ^{13}C NMR spectra and experiments ($\{^{1}H-^{1}H\}$ COSY, $\{^{1}H-^{13}C\}$ HSQC, and DEPT-135) were performed on a 300 MHz Mercury NMR spectrometer. Chemical shifts are given in ppm with respect to tetramethylsilane. Gas chromatography−mass spectrometry (GC−MS) data were obtained using an Agilent Technologies 6890N GC 5975B MSD instrument. Pneumatically assisted electrospray mass spectrometry (ES−MS) spectra were recorded from anhydrous acetonitrile solutions on an Agilent 6520 Q-TOF mass spectrometer by infusion at 0.5 mL/min. Elemental analyses were conducted at Desert Analytics, Inc. (Tucson, AZ). Electronic spectra in the UV/visible range were recorded at 298 K with a Varian Cary 50 Bio UV/visible spectrophotometer with an attached Cary Single Cell Peltier Accessory for temperature control. Fluorescence at 298 K and above was measured on a Varian Cary Eclipse fluorescence spectrophotometer with an attached Quantum Northwest Temperature Control and/or on a Horiba−Jobin−Yvon IBH Fluorolog-3 spectrofluorimeter, equipped with three-slit double-grating excitation and emission monochromators and a continuous-wave 450 W Xe arc lamp as the light source for excitation. Phosphorescence scans (77 K) were taken on a Perkin-Elmer LS50B instrument. During luminescence titrations, a Masterflex L/S compact, variable-speed pump was used with Chem-Durance Bio and Tygon Chemical 2001 tubing to transfer solutions to a 1.0 cm flow cuvette (Starna Cells, Inc.), and a Masterflex L/S Digital Drive with a Masterflex L/S Easy-Load II pump head for precision tubing was used to automatically dispense $Eu(NO_3)_3$ solutions. Luminescence lifetimes were determined with a Horiba−Jobin−Yvon IBH Fluorolog-3 spectrofluorimeter, adapted for time-correlated single-photon-counting (TCSPC) and multichannel scaling (MCS) measurements. A sub-microsecond Xe flashlamp (Jobin Yvon, 5000 XeF) was used as the light source, with an input pulse energy (100 nF discharge capacitance) of ca. 50 mJ, yielding an optical-pulse duration of less than 300 ns at full-width half-maximum. Emission was monitored perpendicularly to the excitation pulse, using either a TBX-04-D (or R928P) detector in the UV/visible region ("S" side) or a Hamamatsu H9170-75 photomultiplier tube (PMT; or C9940-01 PMT) as the NIR detector ("T" side). For measurements in the UV/visible region, spectral selection was achieved by passage through the double-grating emission monochromator (2.1 nm/mm dispersion; 1200 grooves/mm), and the spectra were corrected for emission spectral response (detector and grating). For measurements in the NIR, spectral selection was achieved by passage through a double-grating emission monochromator (600 grooves/nm; 1 μm blaze), and the observed emission in this case was not corrected for the efficiency of the detector or grating. A thermoelectrically cooled single-photon-detection module (Horiba−Jobin−Yvon IBH, TBX-04-D) incorporating a fast-rise-time PMT, a wide-bandwidth preamplifier, and a picosecond constant-fraction discriminator was used as the detector. Signals were acquired with an IBH DataStation Hub photon-counting module in TCSPC mode, and data analysis was performed with the commercially available DAS-6 decay-analysis software package from Horiba−Jobin−Yvon IBH. The goodness of fit was assessed by minimization of the reduced χ^2 function and a visual inspection of the weighted residuals. Each trace contained at least 10 000 points, and the reported lifetime values resulted from at least three independent measurements.

The quantum yields (Φ) were measured by the optically dilute relative method[50] by use of eq 1, where $\int I\,d\lambda$ is the numerically integrated intensity from the luminescence spectra, I is the luminescent intensity at the excitation wavelength, A is the absorbance at the excitation wavelength, and n is the index of refraction of the solution. The subscript R denotes "reference".

$$\frac{\Phi_{sample}}{\Phi_R} = \left(\frac{\int I_{sample}\,d\lambda}{\int I_R\,d\lambda}\right)\left(\frac{I_{R,exc}}{I_{sample,exc}}\right)\left(\frac{A_{R,\lambda_{exc}}}{A_{sample,\lambda_{exc}}}\right)\left(\frac{n_{sample}}{n_R}\right)^2 \quad (1)$$

Quantum yields of the ligand-centered emission were measured relative to quinine sulfate in 0.05 M H_2SO_4 (Q_{abs} = 54.6%).[51] Quantum yields of the metal-centered emission were determined at excitation wavelengths at which (i) the Lambert−Beer law is obeyed and (ii) the absorption of the reference closely matches that of the sample. $Cs_3[Eu(DPA)_3]$ and $Cs_3[Tb(DPA)_3]$ in 0.1 M Tris buffer were used as standards for the Eu^{III}- and Tb^{III}-containing complexes (Q_{abs}= 24.0 and 22.0%),[52] whereas quinine sulfate in 0.05 M H_2SO_4 and ligand **L** in MeCN were used as standards for $[LnL_n]^{3+}$ (Ln^{III} = Nd, Sm, Gd, Dy, Er, and Yb). The complex $[Yb(tta)_3(H_2O)_2]$ (tta = thenoyltrifluoroacetylacetonate; Q_{abs} = 0.35%) in toluene was also used as a standard for $[YbL_n]^{3+}$.[53] $Cs_3[Ln(DPA)_3]$ (Ln^{III} = Eu and Tb) and $[Yb(tta)_3(H_2O)_2]$ were synthesized according to the published methods.[54,55] The estimated error for quantum yields is ±10%.

Luminescence titrations were performed overnight with an automatic titration system where a solution containing 5.0×10^{-5} M **L**, as well as 0.05 M Et_4NClO_4 to maintain ionic strength, was constantly pumped back and forth from a sealed round-bottomed flask and through a 10 mm quartz flow cuvette placed in the cell holder of a Varian Cary Eclipse fluorescence spectrophotometer set to scan every 15−18 min. At consistent time intervals, a solution of 1.0×10^{-3} M $Ln(NO_3)_3$ (Ln^{III} = Eu and Tb) in 0.05 M Et_4NClO_4 was dispensed into the **L** solution by an automatic peristaltic pump designed for precision. For each titration, at least 16 min was allowed for the solution in the flask to homogenize with that in the cuvette as well as to allow for the lanthanide(III) species to equilibrate. Factor analysis and stability constant determinations were carried out with the program *Hyperquad2006*.[56] All data reported are the average of three independent measurements. Computations were run on a Dell Precision 390 using the *Spartan 06* program.[57]

Preparation of $[EuL_3]^{3+}$. A total of 0.097 g of **L** (0.25 mmol) and 0.030 g of $EuCl_3 \cdot 6H_2O$ (0.081 mmol) were added to a 50 mL round-bottomed flask. The mixture powder was then degassed by a vacuum, and the flask was placed under a N_2 atmosphere. A total of 5 mL of anhydrous methanol was added to the flask. The mixture was then stirred vigorously under a N_2 flow until the solution became clear. Liquid N_2 was used to freeze the solution, and once again air was removed by a vacuum. This step was repeated three to five times, and then the flask was filled with N_2 again. The whole mixture was then refluxed under N_2 overnight at 328 K. After evaporation of the solvent and drying of the crude product, the latter was recrystallized by the slow diffusion of *tert*-butyl methyl ether into a concentrated, hot, and anhydrous MeOH solution to give 0.079 g of $[EuL_3]Cl_3$ (71%).

The other $[LnL_3]^{3+}$ complexes [Ln^{III} = Eu, Gd, Tb, and Yb; **L** = (*R*,*R*)-**1** and (*S*,*S*)-**1**] were prepared in 50−71% yield according to the same procedure. Each of the complexes gave satisfactory elemental analyses. These elemental analyses were conducted on samples dried at about 313 K and under reduced pressure. It should be mentioned that a similar synthetic procedure was used to prepare $[LnL_3]^{3+}$ with (*R*,*S*)-**1**, but the elemental analyses suggested the formation of 1:2 species, which were not characterized and studied further because the purpose of this work was to study the formation of tris lanthanide(III) complexes and investigate their photophysical properties in solution.

$[Eu((R,R)\text{-}\mathbf{1})_3]Cl_3$. Yield: 0.091 g, 71%. Anal. Calcd for $C_{69}H_{69}N_9O_6Cl_3Eu$: C, 60.1; H, 5.0; N, 9.1. Found: C, 60.0; H, 4.9; N, 9.2. ES-MS (MeCN): m/z 424.1 ($[Eu((R,R)\text{-}\mathbf{1})_3]^{3+}$).

$[Eu((S,S)\text{-}\mathbf{1})_3]Cl_3$. Yield: 0.064 g, 50%. Anal. Calcd for $C_{69}H_{69}N_9O_6Cl_3Eu$: C, 60.1; H, 5.0; N, 9.1. Found: C, 60.1; H, 5.1; N, 9.3. ES-MS (MeCN): m/z 424.2 ($[Eu((S,S)\text{-}\mathbf{1})_3]^{3+}$).

$[Eu((R,R)\text{-}\mathbf{1})_3](CF_3SO_3)_3$. Yield: 0.095 g, 60%. Anal. Calcd for $C_{72}H_{69}F_3N_9O_{15}S_3Eu$: C, 50.3; H, 4.0; N, 7.3. Found: C, 50.3; H, 3.7; N, 7.3. ES-MS (MeCN): m/z 424.2 ($[Eu((R,R)\text{-}\mathbf{1})_3]^{3+}$).

$[Eu((S,S)\text{-}\mathbf{1})_3](CF_3SO_3)_3$. Yield: 0.082 g, 52%. Anal. Calcd for $C_{72}H_{69}F_3N_9O_{15}S_3Eu$: C, 50.3; H, 4.0; N, 7.3. Found: C, 50.2; H, 3.7; N, 7.3. ES-MS (MeCN): m/z 424.2 ($[Eu((S,S)\text{-}\mathbf{1})_3]^{3+}$).

$[Gd((R,R)\text{-}\mathbf{1})_3]Cl_3$. Yield: 0.085 g, 66%. Anal. Calcd for $C_{69}H_{69}N_9O_6Cl_3Gd$: C, 59.9; H, 5.0; N, 9.1. Found: C, 59.7; H, 4.9; N, 9.0. ES-MS (MeCN): m/z 425.8 ($[Gd((R,R)\text{-}\mathbf{1})_3]^{3+}$).

dx.doi.org/10.1021/ic202094p | *Inorg. Chem.* 2012, 51, 647−660

[Gd((*S*,*S*)-**1**)$_3$]Cl$_3$. Yield: 0.084 g, 65%. Anal. Calcd for $C_{69}H_{69}N_9O_6Cl_3Gd$: C, 59.9; H, 5.0; N, 9.1. Found: C, 59.8; H, 5.1; N, 8.9. ES-MS (MeCN): *m*/*z* 425.9 ([Gd((*S*,*S*)-**1**)$_3$]$^{3+}$).

[Tb((*R*,*R*)-**1**)$_3$]Cl$_3$. Yield: 0.086 g, 66%. Anal. Calcd for $C_{69}H_{69}N_9O_6Cl_3Tb$: C, 59.8; H, 5.0; N, 9.1. Found: C, 59.8; H, 4.8; N, 9.2. ES-MS (MeCN): *m*/*z* 426.2 ([Tb((*R*,*R*)-**1**)$_3$]$^{3+}$).

[Tb((*S*,*S*)-**1**)$_3$]Cl$_3$. Yield: 0.070 g, 54%. Anal. Calcd for $C_{69}H_{69}N_9O_6Cl_3Tb$: C, 59.8; H, 5.0; N, 9.1. Found: C, 59.7; H, 4.9; N, 9.0. ES-MS (MeCN): *m*/*z* 426.1 ([Tb((*S*,*S*)-**1**)$_3$]$^{3+}$).

[Yb((*R*,*R*)-**1**)$_3$]Cl$_3$. Yield: 0.082 g, 63%. Anal. Calcd for $C_{69}H_{69}N_9O_6Cl_3Yb$: C, 59.2; H, 5.0; N, 9.0. Found: C, 59.4; H, 4.9; N, 9.0. ES-MS (MeCN): *m*/*z* 431.2 ([Yb((*R*,*R*)-**1**)$_3$]$^{3+}$).

[Yb((*S*,*S*)-**1**)$_3$]Cl$_3$. Yield: 0.066 g, 51%. Anal. Calcd for $C_{69}H_{69}N_9O_6Cl_3Yb$: C, 59.2; H, 5.0; N, 9.0. Found: C, 59.1; H, 4.7; N, 9.3. ES-MS (MeCN): *m*/*z* 431.3 ([Yb((*S*,*S*)-**1**)$_3$]$^{3+}$).

RESULTS AND DISCUSSION

Structure of L. The synthesis of the three isomers of **L**, namely, (*R*,*R*)-, (*S*,*S*)-, and (*R*,*S*)-**1**, was described in a preliminary report.[36] It was shown that the opposite optical rotation values of (*R*,*R*)-**1** and (*S*,*S*)-**1** (−213.4° and +213.6°, respectively) confirmed the chirality arising from the asymmetric C atoms and the preparation of each enantiomeric form of **L**, while an optical rotation value of −0.8° for (*R*,*S*)-**1** corroborated the synthesis of the meso ligand with high purity. The room-temperature ^{1}H and ^{13}C NMR spectra of the three isomers of **L** in CD_3CN and/or CD_2Cl_2, which display 6 and 10 signals, respectively, are consistent with the presence of a single species having a C_{2v} symmetry: $X^{2,2'}$, $X^{3,3'}$, $X^{6,6'}$, $X^{7,7'}$ (X = C, H), $C^{5,5'}$, and $Ph^{8,8'}$ give rise to only one signal each. This is also corroborated by variable-temperature ^{1}H NMR experiments because the latter do not affect the signals of the various protons present in (*R*,*R*)-**1** and (*R*,*S*)-**1** (Figure S1 in the Supporting Information). The only significant shift observed is for the proton of the NH group moving upfield from ∼8.2 to ∼7.9 ppm with increasing temperature (253−328 K). Finally, the absence of a nuclear Overhauser effect between $H^{3,3'}$ and NH points to a syn,syn,*ZZ* conformation for each isomer of **L**, as was already reported for **L**.[8,58]

This conformation also prevails in the solid state, as evidenced by the X-ray crystal structure of the meso isomer, (*R*,*S*)-**1** (Figure 1). The unit cell contains two independent molecules A and B, the bond lengths and angles of which differ only slightly (Tables 1 and S1 in the Supporting Information). It is worth noting that such a syn,syn,*ZZ* conformation was already observed for 2,6-dicarboxamidopyridine derivatives[58−60] and is driven by the existence of two strong intramolecular hydrogen bonds involving the N atom of the pyridine ring and the NH portion of each carboxamide unit [NH···N(pyridine) = 2.33 and 2.29 Å or 2.34 and 2.35 Å for each independent molecule, respectively]. The importance of these intramolecular hydrogen-bonding interactions is evidenced by the observation of almost coplanar arrangements of the carboxamide side arms with the central pyridine ring [interplanar angles of 3.53(0.16)° and 3.63(0.15)° between C10−C9−O1−N1 or C14−C15−O2−N3 and C10−C14−N2, whereas the other independent molecule shows interplanar angles of 3.83(0.15)° and 6.39(0.14)°, respectively]. Similarly, interplanar angles of 6.03(8) and 12.53(9)° and contact distances of 2.32 and 2.36 Å were reported for **L**,[8,58] whereas ligand **L**[9] showed an average interplanar angle of 24° with intramolecular hydrogen-bonding contact distances of 2.33−2.38 Å.[59] It is worth noting that the structure of (*R*,*S*)-**1** does not reveal that each NH unit of one molecule interacts with one carbonyl O atom of another molecule to form intermolecular hydrogen bonds, as was evidenced for the two 2,6-dicarboxamidopyridine derivatives, **L**[8] and **L**.[9,58,59]

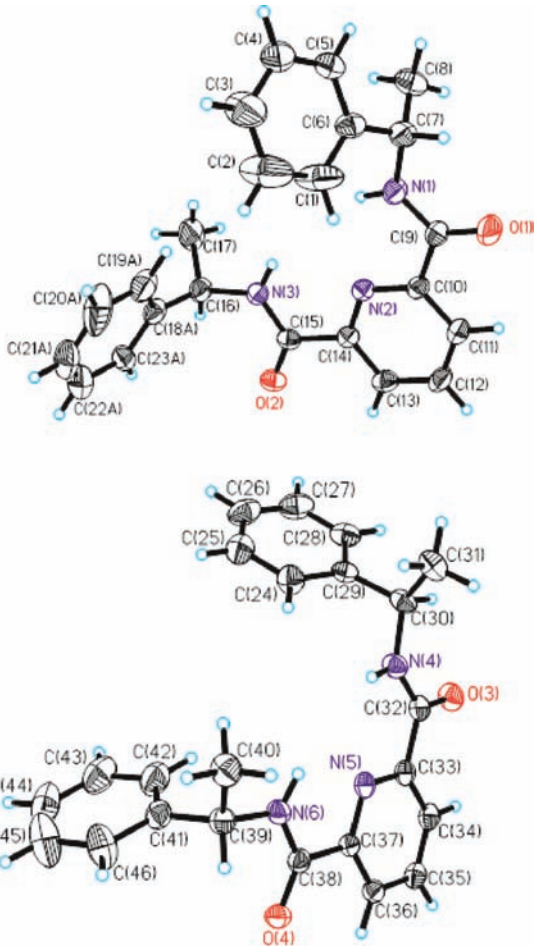

Figure 1. Molecular structure and atom-numbering scheme for the two types of (*R*,*S*)-**1** molecules found in the unit cell. Ellipsoids are represented with 50% probability.

Although we were not able to obtain suitable X-ray-quality single crystals for the other two isomers of **L**, (*R*,*R*)-**1** and (*S*,*S*)-**1**, their conformation predicted from gas-phase density functional theory calculations, utilizing B3LYP[61,62] and the 6-31G(d) basis set,[63,64] pointed to a structural pattern similar to that of the X-ray crystal structure of (*R*,*S*)-**1**, namely, a syn,syn,*ZZ* conformation, and also confirmed the enantiomeric nature of (*R*,*R*)-**1** and (*S*,*S*)-**1** (Figure S2 in the Supporting Information). It is worth noting that the predicted conformation from gas-phase molecular mechanics calculations and the resolved X-ray crystal structure for (*R*,*S*)-**1** are in good agreement with each other (Figures 1 and S2 in the Supporting Information). However, the predicted conformations show that the two carbonyl groups in (*R*,*R*)-**1** and (*S*,*S*)-**1** are bent to opposite sides, whereas the two carboxamide O atoms are on the same side of the pyridine ring for the meso isomer, as evidenced in the X-ray crystal structure and the predicted conformation of (*R*,*S*)-**1**. The position of the carboxamide O atoms in the meso isomer is consistent with that observed in **L**,[8,58] but the interplanar angles are smaller [3.53(0.16) and 3.63(0.15)° or 3.83(0.15)° and 6.39(0.14)° vs 6.03(8) and 12.53(9)°] and point to the fact that the carbonyls are even more in the plane with the pyridine ring than in **L**.[8]

dx.doi.org/10.1021/ic202094p | *Inorg. Chem.* 2012, 51, 647−660

Interaction between L and Ln^{III} Ions. ES-MS spectra were recorded in order to probe the various Ln^{III}-containing species that may be present in solution. Solutions of **L** [2×10^{-3} M in anhydrous MeCN; **L** = (*R*,*R*)-**1**] were titrated with either $Eu(NO_3)_3 \cdot 6H_2O$ or $Eu(CF_3SO_3)_3 \cdot 6H_2O$ at 298 K for ratios $R = [Eu]_t/[L]_t = 0-4$. The spectra suggest the presence of $[LnL_n]^{3+}$ ($n = 1-4$) species, some of them with solvation molecules and/or in the form of nitrate/triflate adducts (Tables 2 and S2 and Figure S3 in the Supporting Information). Nitrate/triflate adducts and isotropic distribution help in identifying the species, as shown in Figure S4 in the Supporting Information. Although ES-MS analysis is only qualitative, it is worth noting that $[LnL_3]^{3+}$ is the most abundant species in the spectra of solutions with small *R* values, whereas solutions with larger *R* values show the coexistence of the latter species with $[LnL_2]^{3+}$ and $[LnL]^{3+}$. These data suggest the presence of the 1:1, 1:2, and 1:3 complexes in solution, as well as a species with four ligands. Such species have been observed for ligands derived from, e.g., pyridine-2,6-dicarboxamide and bis(benzimidazole)-pyridine and were assigned to an outer-sphere association of a fourth ligand molecule with a 1:3 complex.[37,65−67] However, it is most likely that such a species with four ligands is only formed during the ES-MS experiments, as corroborated by the luminescence (no effect on the fitting of the data) and NMR titrations (an excess of ligand only results in the presence of the 1:3 complex and free ligand; see below). More importantly, the ES-MS data indicate the presence of the 1:3 complex in solution because the latter is always observed in an anhydrous acetonitrile solution and also represents the most abundant Ln^{III}-containing species in solution at every *R* value.

Table 2. Species Observed in the ES-MS Spectra of Solutions ($[L]_t = 2 \times 10^{-3}$ M in Anhydrous MeCN; L = (*R*,*R*)-1) with Ratios $R = [Eu]_t/[L]_t = 0-4$ at 298 K

species	m/z^a	species	.
$[(L) + H]^+$	374.2	$[Eu(L)(NO_3)_2]^+$	650.1
$[(L) + Na]^+$	396.2	$[Eu(L)_3(NO_3)]^{2+}$	667.2
$[Eu(L)_3]^{3+}$	424.2	$[2(L) + Na]^+$	769.3
$[Eu(L)_2(NO_3)]^{2+}$	480.6	$[Eu(L)_2(NO_3)_2]^+$	1023.2
$[Eu(L)_4]^{3+}$	548.5	$[Eu(L)_3(NO_3)_2]^+$	1396.4

[a] *m*/*z* values given for the maximum of the peak at unit mass resolution.

To confirm these observations and also to quantitatively characterize the formation of complexes with **L**, luminescence titrations of **L** with $Eu(NO_3)_3 \cdot 6H_2O$ at 298 K in anhydrous MeCN, in the presence of 0.05 M Et_4NClO_4, and under a N_2 atmosphere were performed. Taking account of the species identified in the ES-MS and NMR spectra (see below for an NMR discussion), the luminescence data (Figures S5 and S6 in the Supporting Information) were fitted with nonlinear least-squares methods to equilibria (2)−(4), where solvation and anion coordination were omitted.

$$Eu^{3+} + L \rightleftharpoons [EuL]^{3+} \quad \log \beta_1 \tag{2}$$

$$Eu^{3+} + 2L \rightleftharpoons [EuL_2]^{3+} \quad \log \beta_2 \tag{3}$$

$$Eu^{3+} + 3L \rightleftharpoons [EuL_3]^{3+} \quad \log \beta_3 \tag{4}$$

Although factor analysis indicates the presence of three or four emitting species, a model including $[EuL_4]^{3+}$ does not improve the fit, in agreement with the postulated outer-sphere nature of this species detected in the gas phase. Close examination of the time-resolved luminescence data shows that plots of the luminescence intensity versus the ratio $R = [Eu]_t/[L]_t$ at several wavelengths (Figure S7 in the Supporting Information) have essentially two breaks at $R = 0.33$ and 0.5 (1:3 and 1:2 complexes). The cumulative stability constants are summarized in Table 3.

Table 3. Cumulative Stability Constants of $[Eu(X)_n]^{3+}$ ($n = 1-3$ and X = L and L^i with $i = 4-7$) in Anhydrous MeCN at 293 or 298 K

X	$\log \beta_1$	$\log \beta_2$	$\log \beta_3$
L = (*R*,*R*)-**1**[a]	8.0(2)	15.9(2)	23.8(2)
L^4 [b]	8.2(4)	14.6(5)	19.7(5)
L^5 [c]	8.3(3)	15.3(3)	22.3(3)
L^6 [d]	8.3(6)	13.9(6)	17.6(7)
L^7 [d]	4.9(5)	9.8(6)	

[a] Similar results were obtained for (*S*,*S*)-**1**. [b] Taken from ref 37. [c] Taken from ref 68. [d] Taken from ref 58.

The log β_3 value of the europium(III) complex (23.8) is in good agreement with those reported for corresponding compounds with 2,6-dicarboxamidopyridine derivatives (e.g., 22.3, 19.7, and 17.6 for L^5, L^4, and L^6).[37,58,68] Of special importance, it confirms that the steric hindrances resulting from the wrapping of the tridentate strands play a predominant role in the formation of the triple-helical complexes $[LnL^i_3]^{3+}$ ($i = 5-8$).[58,68] It was shown that the bulkiness of the terminal tertiary amide groups resulted in increased interstrand steric repulsions and, consequently, destabilized significantly the stability of the 1:3 complex (the log β_3 values were lowered by several orders of magnitude) to the point where the formation of this species was not observed.[58] In the latter case, the terminal dibenzylamine groups in L^7 precluded the formation of 1:3 species because of their bulkiness, and only resulted in the observation of 1:1 and 1:2 species. However, the removal of two benzyl groups led to the formation of tris complexes, as evidenced by the crystal structure of $[Tb(L^8)_3]_2(CF_3SO_3)_6$, but it was a slow process in solution because of the existence of several inert conformational isomers resulting from the blocked rotations around the OC−N bonds.[58] This slow complexation process was ascribed from stabilization of the ligand L^8 in its syn,syn,*ZZ* conformation and, as a result, strongly limited its characterization in solution. The replacement of the benzyl groups of the carboxamide units by phenylethyl substituents with respect to L^7 confirmed the formation of tris complexes with **L** [L = (*R*,*R*)-**1** and (*S*,*S*)-**1**] in the solid state (see below) but also in solution (log β_3 of 23.8). This can be attributed to the fact that in L^8 the replacement of one of the two H atoms of the benzyl group by a methyl substituent probably results in a smaller activation energy barrier for rotation about the OC−N bonds (steric hindrances due to the presence of the methyl group) and, therefore, **L** [L = (*R*,*R*)-**1** and (*S*,*S*)-**1**] is not locked into its syn,syn,*ZZ* conformation, as seen for L^8. Thus, the two intramolecular NH···N(pyridine) hydrogen bonds, which led to the formation of a blocked syn,syn,*ZZ* conformation for L^8,[58] are weakened and do not prevent the formation of stable 1:3 complexes with **L** [L = (*R*,*R*)-**1** and (*S*,*S*)-**1**] in solution (a faster complexation reaction is favored), as evidenced by the luminescence titrations and ^1H NMR spectra.

The speciation and, in particular, the formation of stable 1:3 species with **L** [L = (*R*,*R*)-**1** and/or (*S*,*S*)-**1**] in solution under anhydrous conditions were confirmed by monitoring the titration

dx.doi.org/10.1021/ic202094p | Inorg. Chem. 2012, 51, 647−660

of (*R*,*R*)-**1** with La^{III} by ^1H NMR at 298 K (Figure 2). The successive formation of the three complexes, namely, 1:1, 1:2, and 1:3, was observed for ratios $R = [La]_t/[L]_t$, going from 0.33 to 0.5 to 1.0. When *R* reaches 0.33, all ligands are complexed and are in the 1:3 species, whereas the solutions with *R* = 1.0 and 0.5 show the various La^{III}-containing species (1:1 and 1:2, and 1:1, 1:2, and 1:3, respectively). It is worth noting that no free ligand is observed in solution for the various ratios (within the experimental error), confirming the successive formation of the three Ln^{III}-containing compounds with **L**. The addition of more ligands (*R* = 0.2) validated these observations because the ^1H NMR spectrum of this solution only showed the 1:3 species and the excess of free ligand. A similar situation was also observed for Eu^{III} (Figure S8 in the Supporting Information). The observation of only one set of signals for each complex in these ^1H NMR spectra corroborates that **L** [**L** = (*R*,*R*)-**1** and/or (*S*,*S*)-**1**] adopts an anti,anti conformation upon complexation to the Ln^{III} ions but also that the solution contains only one major diastereoisomer of $[LnL_3]^{3+}$ (either Λ-$[Ln((R,R)\text{-}\mathbf{1})_3]^{3+}$ or Δ-$[Ln((S,S)\text{-}\mathbf{1})_3]^{3+}$; see below for further details), as was already seen in several other studies on complexes with, i.e., chiral terdendate ligands derived from terpyridine ($\mathbf{L^1}$), bis(benzimidazole)pyridine ($\mathbf{L^2}$ and $\mathbf{L^3}$), or pyridine-2,6-dicarboxamide ($\mathbf{L^4}$ and **L′**) and chiral octadentate 1-hydroxy-2-pyridinone- and 2-hydroxyisophthalamide-based ligands.[37,39,65,69−71] A similar conclusion was also drawn from the CPL measurements.[36,38] It was found that the strong CPL activity exhibited by $[EuL_3]^{3+}$ [e.g., the g_{lum} value amounted to −0.19 at 590 nm for **L** = (*R*,*R*)-**1**] is comparable when either a direct excitation of the Eu^{III} ion in the spectral range of the $^5D_0 \rightarrow {}^7F_1$ transition or an indirect excitation through the ligand absorption bands was used but also is independent of polarization of the excitation beam (e.g., right-, left-, or plane-polarized light). This was consistent with the presence of only one diastereomeric species in solution.[27,28,38,71,72] On the other hand, one would have expected that the CPL would have been dependent on the excitation polarization if the solution would have contained a mixture of diastereoisomers.[73,74] This is also in good agreement with the X-ray crystal structures of $[LnL_3]^{3+}$ [Ln^{III} = Eu, Gd, Tb, and Yb; **L** = (*R*,*R*)-**1** and (*S*,*S*)-**1**] showing the formation of triple-helical complexes in the solid state (see below). In summary, the apparent easy formation of the 1:3 species contrasts with that observed with $\mathbf{L}^{8}$ [58] and confirms that **L** is not blocked in the syn,syn,*ZZ* conformation. Additionally, these ^1H NMR experiments confirmed that a solution of the 1:3 species can be prepared in situ by mixing a MeCN solution of the Ln^{III} salt with one of **L** in a Ln^{III}/**L** molar ratio of 1:3 and under anhydrous conditions.

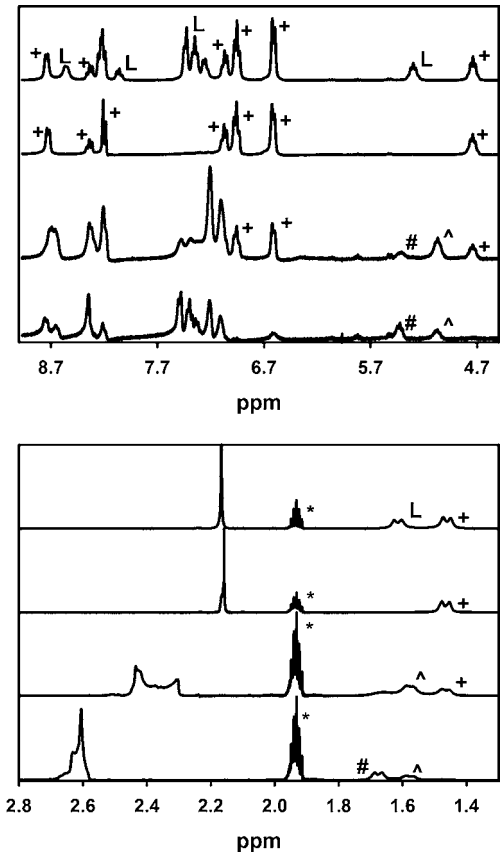

Figure 2. ^1H NMR spectra of solutions containing various ratios $R = [La]_t/[L]_t$ of 0.2, 0.33, 0.5, and 1.0 (from top to bottom) in anhydrous CD_3CN (* symbol) at 298 K. The symbols **L**, #, ^, and + denote signals arising from the **L**, 1:1, 1:2, and 1:3 species, respectively. **L** = (*R*,*R*)-**1**.

Isolation, Characterization, and Structure of $[LnL_3]^{3+}$. The 1:3 complexes were obtained under the form of microcrystalline powders in 50−71% yield from the diffusion of *tert*-butyl methyl ether into concentrated, hot, and anhydrous MeOH solutions containing **L** [**L** = (*R*,*R*)-**1** and (*S*,*S*)-**1**] and $LnX_3{\cdot}xH_2O$ (Ln^{III} = Eu, Gd, Tb, and Yb; $X = Cl^-$, NO_3^-, and/or $CF_3SO_3^-$; *x* = 5 or 6) in a molar ratio of 3.1:1. The isolated $[LnL_3]^{3+}$ complexes (Ln^{III} = Eu, Gd, Tb, and Yb) yielded good elemental analysis, and dissolution in anhydrous MeCN gave ES-MS and/or ^1H NMR data similar to those obtained from complex solutions prepared in situ with a Ln^{III}/**L** molar ratio of 1:3 or 1:5. It is worth noting that the high-resolution $^5D_0 \leftarrow {}^7F_0$ excitation spectra of the Eu^{III}-containing complex solution formed in situ under nonanhydrous conditions confirmed that the Eu^{III} ions were in the form of the 1:3 species in a 6.67×10^{-3} M MeCN solution with a stoichiometric 1:5 ratio.[36] Taking account of these observations, some of the $[LnL_3]^{3+}$ (Ln^{III} = Pr, Nd, Sm, Dy, Er, and Tm) complexes were not isolated but only prepared in situ using anhydrous conditions for the purpose of the photophysical studies. These solutions were prepared in the glovebox using a Ln^{III}/**L** ratio of 1:5 to ensure that only the 1:3 complex species was present in solution because it was observed in a previous study that a ratio of 1:3 resulted in the presence of 1:2 and 1:3 complex species in solution when nonanhydrous conditions were used.[36]

Single crystals suitable for X-ray diffraction analysis were obtained for the $[LnL_3]^{3+}$ (Ln^{III} = Eu, Gd, Tb, and Yb) complexes with the two enantiomeric forms of **L**, (*R*,*R*)-**1** and (*S*,*S*)-**1**. The details of the crystallographic data collection are summarized in Tables 1 and S3 and S4 in the Supporting Information. All complexes are isostructural and crystallize in the cubic space group *I*23. The unit cell contains isolated $[LnL_3]^{3+}$ cations with disordered noncoordinated solvent molecules and chloride anions, which explain the fractional values found (see the Experimental Section). All Ln^{III} ions are coordinated by six carboxamide O atoms and three pyridine N atoms. The structures of the different $[LnL_3]^{3+}$ [Ln^{III} = Eu, Gd, Tb, and Yb; **L** = (*R*,*R*)-**1** and (*S*,*S*)-**1**] cations with the atom-numbering scheme are displayed in Figures 3 and 4 and S9 and S10 in the Supporting Information, and selected bond lengths and angles are reported in Tables 4 and S5−S10 in the Supporting Information, while selected interplanar angles are listed in Table S11 in the Supporting Information. In each

dx.doi.org/10.1021/ic202094p | *Inorg. Chem.* 2012, 51, 647−660

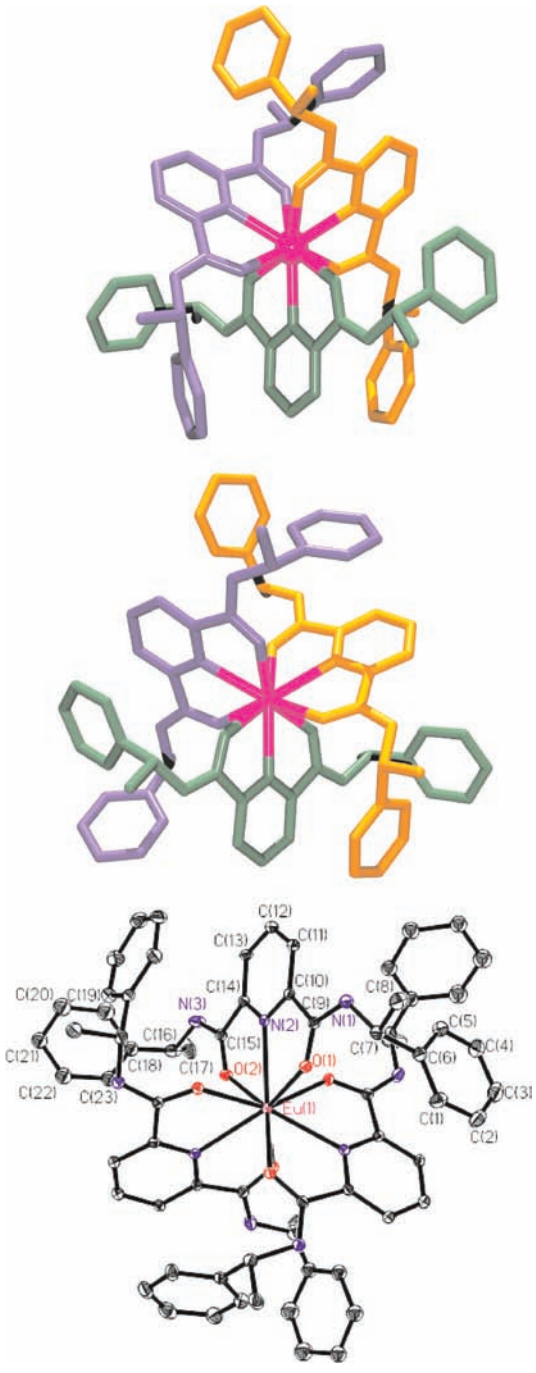

Figure 3. Structures of the Λ-[Eu((*R*,*R*)-**1**)$_3$]$^{3+}$ (top) and Δ-[Eu((*S*,*S*)-**1**)$_3$]$^{3+}$ (middle) cations and atom-numbering scheme for Λ-[Eu((*R*,*R*)-**1**)$_3$]$^{3+}$ (bottom). Ellipsoids are represented with 50% probability.

cation, the three ligand molecules are meridionally coordinated to and in a helical way around the Ln^{III} ion, leading to the observation of almost ideal D_3-like complexes for the four Ln^{III}-containing species. This is corroborated by equivalent Ln−X bond lengths and X−Ln−Y angles (X = N and O; Y = N and O) for each of the three ligand molecules coordinated to the Ln^{III} cation. It is worth noting that the average Ln−X distances become shorter along the studied Ln^{III} ion series (Eu−Yb). For instance, the Ln−N(pyridine) distance in [Ln**L**$_3$]$^{3+}$ is decreasing from 2.564(2), 2.543(2), 2.528(2), to 2.467(2) Å for Ln^{III} = Eu, Gd, Tb, and Yb and **L** = (*R*,*R*)-**1**, respectively.

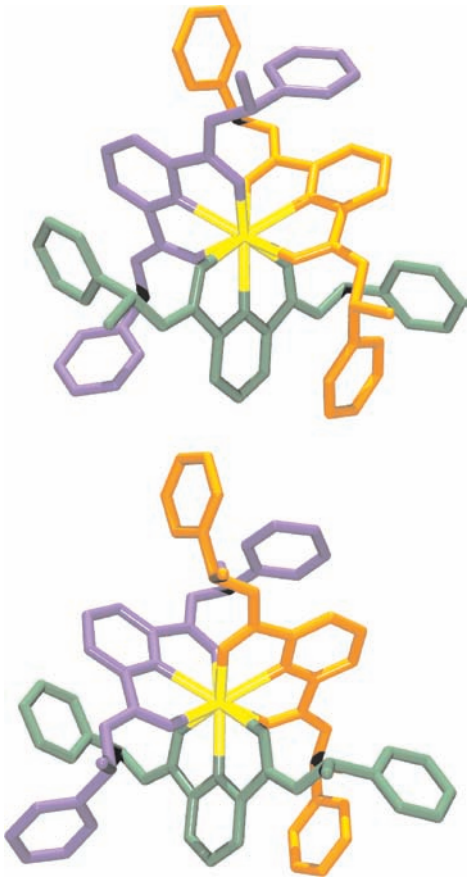

Figure 4. Structures of the Λ-[Yb((*R*,*R*)-**1**)$_3$]$^{3+}$ (top) and Δ-[Yb((*S*,*S*)-**1**)$_3$]$^{3+}$ (bottom) cations.

A similar pattern was observed for the 1:3 species with the other enantiomeric form of **L**, (*S*,*S*)-**1**. One can conclude from these observations that the coordination cavity is modular and fits Ln^{III} ions of various sizes such as Eu^{III} or Yb^{III}. Both X-ray crystal structures of Eu^{III} and Yb^{III} only show slight differences in the interplanar angles between the carboxamide side arms and the central pyridine ring [5.86(0.12) and 7.35(0.16)° vs 4.16(0.12) and 6.75(0.14)° for **L** = (*R*,*R*)-**1**], whereas the angles between the ligand strand planes are very similar (75.28 vs 76.76°), respectively. It is also evidenced by the slightly smaller values of the effective ionic radius (1.09, 1.08, 1.07, and 1.01) of the Ln^{III} ions [Ln = Eu, Gd, Tb, and Yb; **L** = (*R*,*R*)-**1** and (*S*,*S*)-**1**], calculated according to Shannon's definition with r(N) = 1.46 Å and r(O) = 1.31 Å,[75] from the expected ionic radii for 9−coordinate Ln^{III} ions (1.12, 1.07, 1.095, and 1.042 Å), respectively. These smaller values are due to a slight contraction of the Ln^{III} coordination sphere, which is induced by the wrapping of the three tridentate ligand molecules, as was already reported for [Eu**L**$^5_3$]$^{3+}$ (1.09 vs 1.12 Å).[68]

Moreover, the average Ln−N(pyridine) and Ln−O(amide) bonds of 2.56 or 2.54 and 2.40 or 2.38 Å are close to those found in the related lanthanide(III) complexes (Ln = Eu and Tb) with carboxamide ligand derivatives, respectively.[68,76] The crystal packing is governed by intramolecular (C1−C6 phenyl ring with the C10−C14−N2 central pyridine ring of another ligand strand, but in the same complex molecule) and intermolecular (C1−C6 phenyl ring with the C18−C23 phenyl ring of another complex molecule) π-stacking interactions and weak intermolecular hydrogen-bonding interactions between

dx.doi.org/10.1021/ic202094p | *Inorg. Chem.* 2012, 51, 647−660

Table 4. Selected Bond Lengths (Å) and Angles (deg) in $[LnL_3]^{3+}$ (Standard Deviation in Parentheses)

	Bond Lengths					
	$[EuL_3]^{3+}$ [L = (*R*,*R*)-**1**)]			$[YbL_3]^{3+}$ [L = (*R*,*R*)-**1**)]		
	ligand	ligand #1	ligand #2	ligand	ligand #1	ligand #2
Ln1−N2	2.564(2)	2.564(2)	2.564(2)	2.467(2)	2.467(2)	2.467(2)
Ln1−O1	2.397(2)	2.397(2)	2.397(2)	2.319(2)	2.319(2)	2.319(2)
Ln1−O2	2.397(2)	2.397(2)	2.397(2)	2.333(2)	2.333(2)	2.333(2)
Bite Angles N−Ln−N, O−Ln−N, and O−Ln−O						
N2−Ln1−N2#1		119.9(1)			120.0(1)	
N2−Ln1−N2#2		119.9(1)			120.0(1)	
N2#1−Ln1−N2#2		119.9(1)			120.0(1)	
O1−Ln1−N2#1		69.6(1)			138.5(1)	
O2−Ln1−N2#1		140.5(1)			69.8(1)	
O1−Ln1−N2#2		136.6(1)			72.8(1)	
O2−Ln1−N2#2		76.0(1)			137.6(1)	
O1#1−Ln1−N2		136.6(1)			72.7(1)	
O2#1−Ln1−N2		76.0(1)			137.6(1)	
O1#1−Ln1−N2#2		69.6(1)			138.5(1)	
O2#1−Ln1−N2#2		140.5(1)			69.8(1)	
O1#2−Ln1−N2		69.6(1)			138.5(1)	
O2#2−Ln1−N2		140.5(1)			69.8(1)	
O1#2−Ln1−N2#1		136.6(1)			72.7(1)	
O2#2−Ln1−N2#1		76.0(1)			137.6(1)	
O1−Ln1−O1#1		81.6(1)			79.9(1)	
O1−Ln1−O1#2		81.6(1)			79.9(1)	
O1−Ln1−O2#1		82.7(1)			142.6(1)	
O1−Ln1−O2#2		145.5(1)			83.9(1)	
O2−Ln1−O1#1		145.5(1)			83.9(1)	
O2−Ln1−O1#2		82.7(1)			142.6(1)	
O2−Ln1−O2#1		82.1(1)			81.1(1)	
O2−Ln1−O2#2		82.1(1)			81.1(1)	
O1#1−Ln1−O1#2		81.6(1)			79.9(1)	
O1#1−Ln1−O2#2		82.7(1)			142.6(1)	
O2#1−Ln1−O1#2		145.5(1)			83.9(1)	
O2#1−Ln1−O2#2		82.1(1)			81.1(1)	

the Cl atom of the noncoordinated chlorides and the amide H atom or the O atom of the noncoordinated solvent molecules (Figure S).

Finally, it should be added that the asymmetric C atoms of the ligands retain their absolute configuration *R* or *S* in all of the complex cations. Thus, the Δ or Λ metal stereochemistry is induced by the chiral nature of the ligand molecules in all of the complexes studied by X-ray crystallography. That is, ligand (*S*,*S*)-**1** induces a Δ chirality about the Ln^{III} ions, whereas ligand (*R*,*R*)-**1** induces a Λ chirality about the Ln^{III} ions. These findings, which confirm the diastereomeric nature of $[LnL_3]^{3+}$ with (*R*,*R*)-**1** and (*S*,*S*)-**1**, are also in agreement with those reported for related highly symmetrical isostructural chiral 1:3 lanthanide(III) complexes with a chiral pyridyldiamide ligand derivative, pyridine-2,6-dicarboxylic acid bis[(1-naphthalen-1-ylethyl)amide] (**L′**). This ligand only differs from **L** by its carboxamide moieties, in which the phenyl groups of **L** are replaced by naphthalene substituents.[39] It is also worth noting that the diastereomeric nature of $[LnL_3]^{3+}$ with (*R*,*R*)-**1** and (*S*,*S*)-**1** also prevails in solution, as evidenced by the CPL results from the Eu^{III}-containing species (observation of mirror-image CPL spectra that are independent of polarization of the excitation beam and whether a direct or an indirect excitation is used).[36,38] A complete study of the chiroptical properties of these compounds of interest will be described in a forthcoming publication.[77]

Ligand-Centered Emission. The electronic spectrum of **L** in solution displays a broad band defined by two broad maxima around 276 and 284 nm and assigned to n → π* and π → π* transitions centered on the pyridinedicarboxamide units (Figure S11 in the Supporting Information). UV irradiation of **L** at room temperature yields one broad unresolved fluorescence band, centered around 337 nm and originating from the $^1\pi\pi^*$ state (Figure 6). At 77 K, the fluorescent band is more structured and emission from the $^3\pi\pi^*$ state appears with a maximum around 391 nm. As one would expect, the findings for both enantiomeric forms of **L**, (*R*,*R*)-**1**, and (*S*,*S*)-**1**, are identical within experimental error. Thus, we only report the photophysical data for one of them thereafter, with **L** meaning either (*R*,*R*)-**1** or (*S*,*S*)-**1**. The same practice is applied to the discussion of the photophysical properties of the $[LnL_3]^{3+}$ complexes.

Upon complexation to Gd^{III} in the 1:3 complex, the broad band observed in the electronic spectrum of **L** is only slightly red-shifted, with the appearance of two broad maxima around 277 and 286 nm. Similar results were obtained for the other $[LnL_3]^{3+}$ complexes investigated (Figure S11 in the Supporting Information). Upon complexation to the nonluminescent Gd^{III} ion, the transitions of the $^1\pi\pi^*$ and $^3\pi\pi^*$ states are red-shifted by 175 and 885 cm^{-1}, respectively (frozen MeCN solution, 77 K; see Figure 6). These changes in the position of the $^1\pi\pi^*$ and $^3\pi\pi^*$ states between the free and complexed ligands

dx.doi.org/10.1021/ic202094p | Inorg. Chem. 2012, 51, 647−660

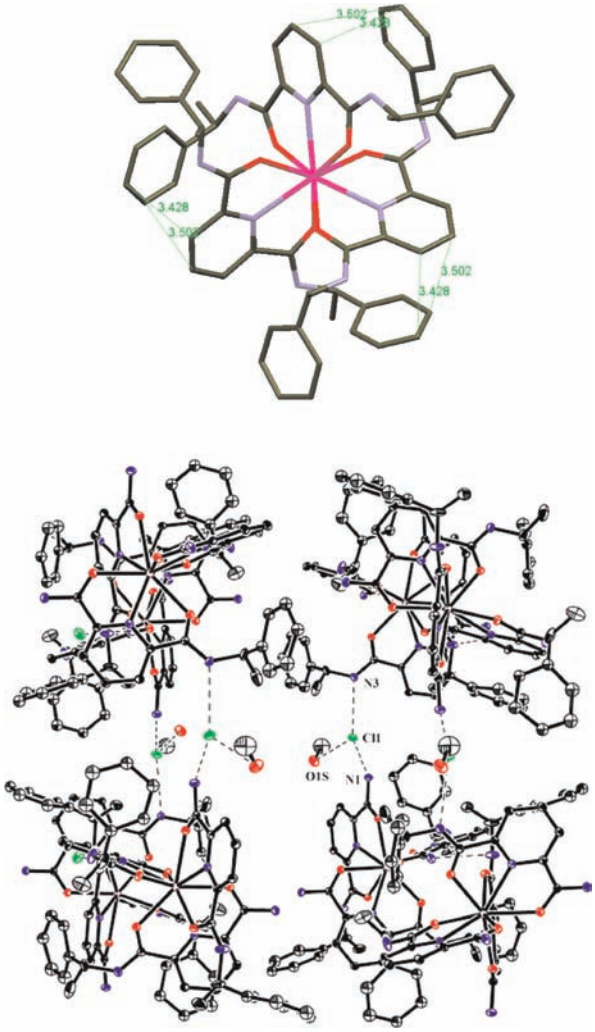

Figure 5. Example of π-stacking interactions (top) and hydrogen-bonding interactions (bottom) observed in the crystal structure of the Λ-$[Eu((R,R)\text{-}\mathbf{1})_3]^{3+}$ cation. The distances for the Cl^- anion hydrogen-bonded to N1, N3, and O1S are 3.172, 3.162, and 3.133 Å, respectively. Ellipsoids are represented with 50% probability.

confirm the formation of the complex. On the other hand, one can also envision that localization of the 0-phonon of the $^3\pi\pi^*$ state of the complexed ligand in the Gd^{III}-containing compound at 27 025 cm^{-1} (or 370 nm) is well suited to sensitize many Ln^{III} ions, emitting, for instance, in the visible (Eu and Tb), NIR (Nd and Yb), or both regions (Pr, Sm, Dy, Er, and Tm).

Eu- and Tb-Centered Luminescence. The luminescence spectra of $[Eu\mathbf{L}_3]^{3+}$ and $[Tb\mathbf{L}_3]^{3+}$ were recorded in MeCN solutions at a concentration of 10^{-3} M, which represents a compromise between decomplexation and self-quenching. According to the stability constants determined for $[Eu\mathbf{L}_n]^{3+}$ in MeCN (n = 1−3; Table 3), about 99% of the species present in solution for a stoichiometric ratio Eu/**L** of 1:3 is under the form of $[Eu\mathbf{L}_3]^{3+}$ (ligand speciation).

Excitation via the ligand-centered n,$\pi \rightarrow \pi^*$ transitions of $[Eu\mathbf{L}_3]^{3+}$ and $[Tb\mathbf{L}_3]^{3+}$ result in the observation of the typical luminescence spectra of Eu^{III} and Tb^{III} with sharp-line emission bands arising from the $^5D_0$ and $^5D_4$ excited states on the ^7F_J manifold ground states (J = 0−6 and 6−0, respectively; Figure 6). It can been seen that the luminescence spectra of $[Eu\mathbf{L}_3]^{3+}$ and $[Tb\mathbf{L}_3]^{3+}$ also show the residual emission of the ligand-centered

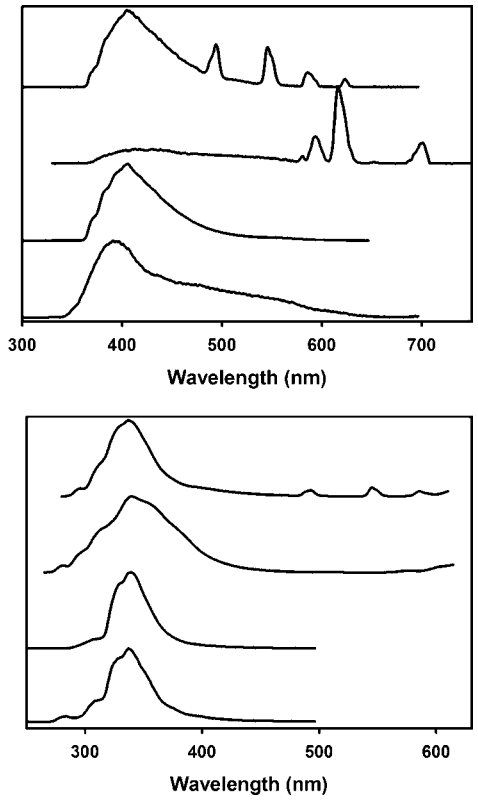

Figure 6. Time-resolved (top) and steady-state (bottom) luminescence spectra of **L** and $[Ln\mathbf{L}_3]^{3+}$ in the solid state at 77 K (frozen MeCN solution) and in a MeCN solution at room temperature and recorded with time delays of 0.0 and 0.1 ms, respectively. From top to bottom: $[Ln\mathbf{L}_3]^{3+}$ (Ln^{III} = Tb, Eu, and Gd) and **L**.

$^1\pi\pi^*$ and $^3\pi\pi^*$ states, suggesting incomplete intersystem crossing (ISC) and ligand-to-Ln^{III} energy transfers, respectively. These poor energy conversion processes are confirmed by the relatively modest-to-small quantum yields of both the ligand- and metal-centered luminescence measured at room temperature, and the ratio between the integrated $^3\pi\pi^*$ and $^1\pi\pi^*$ state emissions, I^T/I^S for the free ligand and its gadolinium(III) complex at 77 K.

The quantum yield of $[Gd\mathbf{L}_3]^{3+}$ (Φ^F = 2.2%) decreases by a factor of 10 with respect to that of the free ligand (Φ^F = 21.2%), whereas the ligand-centered phosphorescence increases, as indicated by the 10-fold increase of I^T/I^S from 4.0×10^{-3} to 4.7×10^{-2} upon complexation of **L** with Gd^{III}. This better ISC efficiency in the gadolinium(III) complex may result from a more favorable energy gap between the $^1\pi\pi^*$ and $^3\pi\pi^*$ states, $\Delta E(^3\pi\pi^* - {}^1\pi\pi^*)$ = 5070 cm^{-1}, as compared to 4190 cm^{-1} in the free ligand [an optimal ISC energy-transfer process needs to have a $\Delta E(^3\pi\pi^* - {}^1\pi\pi^*)$ greater than 5000 cm^{-1}],[78] and from the mixing of the ligand-centered $^1\pi\pi^*$ and $^3\pi\pi^*$ wave functions promoted by spin−orbit and/or paramagnetic effects.[79,80]

The overall quantum yield of the Ln^{III}-centered luminescence obtained upon ligand excitation, Φ^{Ln}_L, amounts to 1.0% for $[Eu\mathbf{L}_3]^{3+}$, compared to 8.6% for the corresponding compound with Tb^{III}. This 9-fold difference may be explained by the fact that (i) Eu^{III} has a tendency to favor the quenching of the singlet excited state of the sensitizing chromophore (a process usually not observed for Tb^{III} since it is very difficult to reduce this ion), (ii) the possibility of having an energy transfer in the

dx.doi.org/10.1021/ic202094p | Inorg. Chem. 2012, 51, 647−660

terbium(III) compounds from the ligand triplet state to a higher metal electronic state (i.e., $^5D_3$) than the emissive state of Tb^{III}, $^5D_4$ (the higher metal state is populated and then undergoes a rapid internal conversion and vibrational relaxation to the emissive metal state $^5D_4$), and (iii) a better efficiency of the ligand-to-metal energy transfer.[81,82] The energy gap between the $^3\pi\pi^*$ state of the complexed ligand and the excited state of Tb^{III}, $^5D_4$, is closer, although relatively large ($\Delta E(^3\pi\pi^*-^5D_4)$ = 6535 cm^{-1}), to the ideal value of 2500–3500 cm^{-1} for an efficient ligand-to-metal energy transfer[78] than the one for $[EuL_3]^{3+}$ ($\Delta E(^3\pi\pi^*-^5D_0)$ = 9800 cm^{-1}). One can conclude that the small quantum yields of the Ln^{III}-centered luminescence clearly point to the poor efficiency of the ISC and ligand-to-metal energy transfers. Another factor that may also largely contribute to relatively modest quantum yields of the europium(III) and terbium(III) complexes is the weak efficiency of the luminescence sensitization by the ligand (η_{sens} = 4.0 × 10^{-5}; see the Supporting Information for a detailed determination of this value). However, the slight decrease in the Eu($^5D_0$) and Tb($^5D_4$) lifetimes from 1.84 and 1.95 to 1.75 and 1.89 ms between 77 K and room temperature suggests that temperature-dependent quenching mechanisms (e.g., energy back transfer, ligand-to-metal charge transfer, or other intermolecular interactions, etc.) do not significantly contribute to the nonradiative deactivation processes responsible for the fairly small Ln^{III}-centered luminescence quantum yields of $[EuL_3]^{3+}$ and $[TbL_3]^{3+}$. The long Eu($^5D_0$) and Tb($^5D_4$) lifetimes also suggest that the metallic site in $[EuL_3]^{3+}$ and $[TbL_3]^{3+}$ is efficiently protected from external interactions (e.g., no solvent molecules present in the first coordination sphere) because of the helical arrangement of the three ligand molecules around the Ln^{III} ion. This is in line with the NMR data because the latter do not point to a partial decomplexation of one of the arms of the coordinated ligand molecules through the binding of a solvent molecule. A similar phenomenon was reported for MeCN solutions of analogous 1:3 complexes with a ligand derived from pyridine-2,6-dicarboxamide (L^4) for which Eu($^5D_0$) and Tb($^5D_4$) lifetime values of 1.58 and 1.55 ms were observed.[37] It is interesting to note that the quantum yields for $[Eu(L)_3]^{3+}$ and $[Tb(L)_3]^{3+}$ are 4.5 and 7.2 times larger than those for $[Ln(L^4)_3]^{3+}$ (0.22 and 1.2%) despite larger $\Delta E(^3\pi\pi^*-^5D_0)$ and $\Delta E(^3\pi\pi^*-^5D_4)$ energy gaps (9800 and 6535 vs 8000 and 4850 cm^{-1}). This can be explained by the fact that L^4 itself is essentially nonluminescent and is only weakly luminescent in the compounds with La and Lu (Φ^F = 5.5 × 10^{-2} and 6.5 × 10^{-2}%),[37] whereas the quantum yields of L and its gadolinium(III) complex amount to 21.2 and 2.2%, respectively. It is also worth pointing out that the Ln-containing compounds with ligands incorporating carboxamide moieties generally exhibit weaker luminescence than those with carboxylic groups. In addition to the effect on the electronic and structural properties, the carboxamide–carboxylate substitution significantly affects the efficiency of the energy-transfer processes and, in particular, the sensitization process. Although a generalization would be difficult, it seems that the latter is improved in systems containing carboxylate groups.[58,67,68,83]

Pr-, Nd-, Sm-, Dy-, Er-, Tm-, and Yb-Centered Luminescence. Because the ligand triplet-excited-state energy seems well suited to populate most of the Ln^{III} ions, we prepared all of the complexes $[LnL_3]^{3+}$ with the Ln^{III} cations emitting from the f–f orbitals and yielding sensitization of Pr, Nd, Sm, Dy, Er, Tm, and Yb. With the exception of Nd and Yb, which only emit in the NIR region, all of them possess transitions in the visible and NIR regions. The luminescence spectra for complexes $[LnL_3]^{3+}$ (Ln^{III} = Pr, Nd, Sm, Dy, Er, Tm, and Yb) are plotted in Figure 7. The luminescence quantum yields and lifetimes in MeCN solutions were measured, when possible, and are discussed thereafter. Below we discuss briefly the feature of these visible- and NIR-emitting lanthanide(III) complexes. It is worth mentioning that the assignment of the Ln^{III}-centered visible and NIR luminescence bands of the systems of interest is consistent with what one would expect from such Ln^{III}-containing compounds.[7,84]

Luminescence spectra of $[NdL_3]^{3+}$ and $[YbL_3]^{3+}$ after excitation into the ligand-centered n,$\pi \rightarrow \pi^*$ transitions display typical narrow band emission in the NIR region. Three characteristic emission bands are observed for $[NdL_3]^{3+}$ at about 890, 1056, and 1340 nm, which correspond to the $^4F_{3/2} \rightarrow {}^4I_J$ (J = $^9/_2$, $^{11}/_2$, and $^{13}/_2$) f–f transitions of the Nd^{III} ion. Similarly, one structured band and one broad emission band are observed for $[YbL_3]^{3+}$ and $[ErL_3]^{3+}$ around 977 and 1511 nm, corresponding to the $^2F_{5/2} \rightarrow {}^2F_{7/2}$ and $^4I_{13/2} \rightarrow {}^4I_{15/2}$ transitions of Yb^{III} and Er^{III}, respectively. It is worth noting that observation of a structured emission band for $[YbL_3]^{3+}$ may be attributed to the crystal-field or stark splitting, as was already reported for other Yb^{III}-based systems.[85–88] Although Er^{III} is known for having visible emission bands,[7] the luminescence spectrum of $[ErL_3]^{3+}$ in the visible region is dominated by the broad emission from the complexed ligand. It is worthwhile to note that the luminescence spectra of $[LnL_3]^{3+}$ (Ln^{III} = Pr, Sm, Dy, and Tm) reveal the characteristic emission bands of Pr^{III}, Sm^{III}, Dy^{III}, and Tm^{III} in the visible and NIR regions upon excitation via the ligand-centered n,$\pi \rightarrow \pi^*$ transitions.[7] The assignment of the emission observed from the $[PrL_3]^{3+}$ complex is more complicated compared with other Ln^{III} ions because Pr^{III} can emit from three different excited states, namely, the $^3P_0$, $^1D_2$, and $^1G_4$ levels. Accordingly, the luminescence spectrum of $[PrL_3]^{3+}$ shows the characteristic visible emission bands of Pr^{III} at about 488, 604, and 650 nm, which can be attributed to the $^3P_0 \rightarrow {}^3H_4$, $^1D_2 \rightarrow {}^3H_4$, and $^3P_0 \rightarrow {}^3F_2$ transitions. The presence of the luminescence peaks of $^1D_2 \rightarrow {}^3H_4$ (604 nm) and $^3P_0 \rightarrow {}^3F_2$ (650 nm) in the spectrum of $[PrL_3]^{3+}$ confirms that the ligand triplet-excited-state energy is relatively well positioned to populate the $^3P_0$ level of Pr^{III}, which is located at about 21 000 cm^{-1} (or 476 nm). This is in line with other published data for which the absence of these two luminescence peaks led to the conclusion that the position of the $^3\pi\pi^*$ state of the ligand in the praseodymium(III) complexes was too low to populate the $^3P_0$ level of Pr^{III} effectively.[89,90] Thus, the visible luminescence spectra of these Pr^{III}-containing compounds only showed the emission band of the $^3P_0 \rightarrow {}^3H_4$ transition at about 490 nm. On the other hand, the observed NIR emission bands in the luminescence spectrum of $[PrL_3]^{3+}$ at 1028 and 1450 nm can be assigned to the $^1D_2 \rightarrow {}^3F_4$ and $^1D_2 \rightarrow {}^1G_4$ transitions.[91] Under the same conditions, the luminescence spectrum of $[SmL_3]^{3+}$ displays the typical visible $^4G_{5/2} \rightarrow {}^6H_{5/2}$, $^6H_{7/2}$, $^6H_{9/2}$, and $^6H_{11/2}$ and NIR $^4G_{5/2} \rightarrow {}^6F_{5/2}$, $^6F_{7/2}$, and $^6F_{9/2}$ transitions centered at 561, 603, 644, and 710 nm and 950, 1030, and 1206 nm, respectively. Although the luminescence of $[TmL_3]^{3+}$ is very weak, the characteristic Tm^{III} emission from the $^1G_4$ level is observed with the visible $^1G_4 \rightarrow {}^3H_6$ and $^3H_4$ (478 and 650 nm) and NIR $^1G_4 \rightarrow {}^3F_4$ transitions (1125 nm). Finally, the luminescence spectrum of $[DyL_3]^{3+}$ displays the characteristic visible (480, 573, and 660 nm) and NIR (1000, 1148, and 1310 nm) emission bands, corresponding to the

dx.doi.org/10.1021/ic202094p | Inorg. Chem. 2012, 51, 647–660

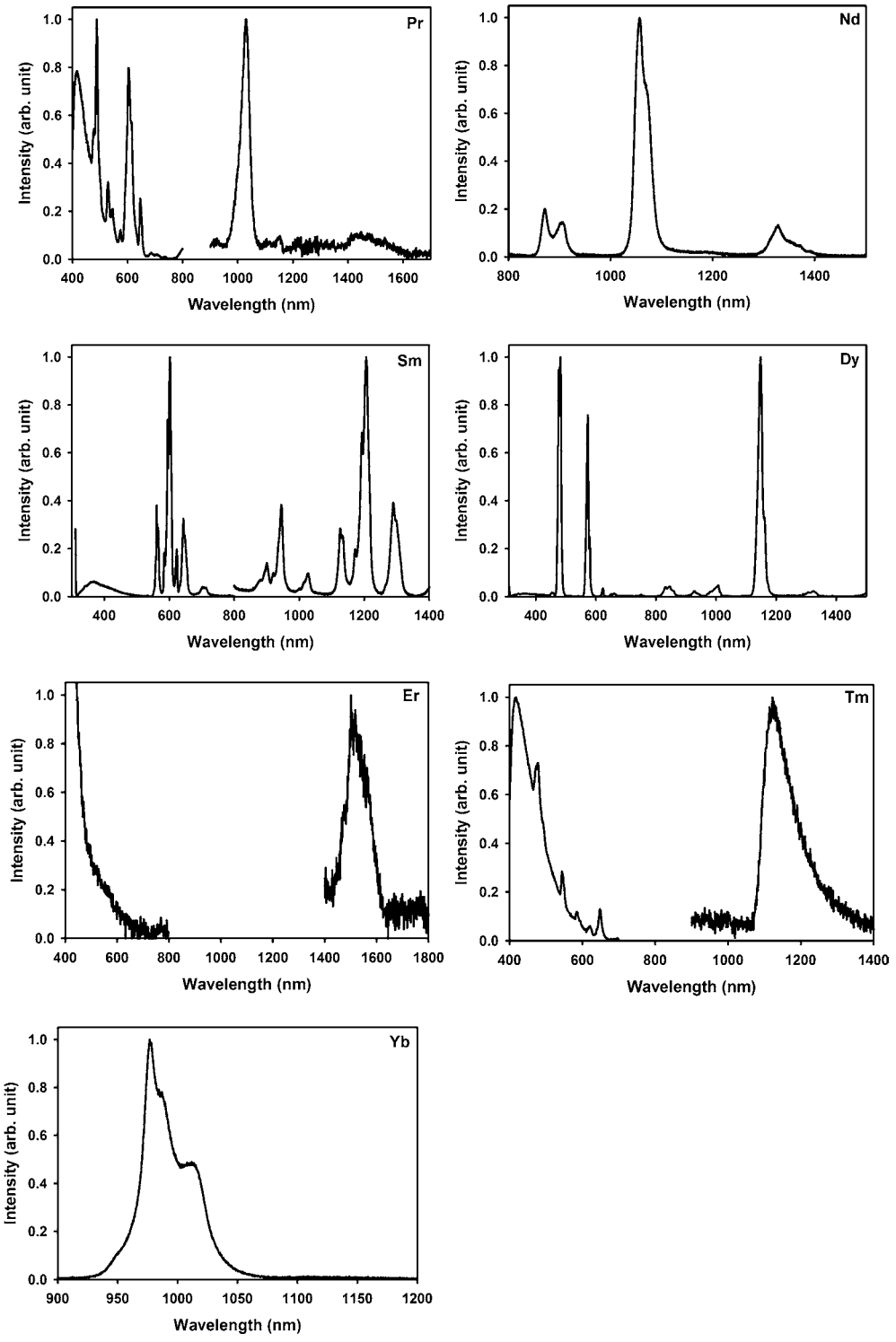

Figure 7. Visible and NIR luminescence spectra of $[LnL_3]^{3+}$ (Ln^{III} = Pr, Nd, Sm, Dy, Er, Tm, and Yb) in 6.7×10^{-3} M anhydrous MeCN at room temperature after excitation into the ligand-centered n,$\pi \rightarrow \pi^*$ transitions (λ_{exc} = 308 nm).

$^4F_{9/2} \rightarrow {}^6H_J$ ($J = {}^{15}/_2$, ${}^{13}/_2$, ${}^{11}/_2$, and ${}^{9}/_2$) and $^4F_{5/2} \rightarrow {}^6F_J$ ($J = {}^{3}/_2$ and ${}^{1}/_2$) transitions, respectively.

Furthermore, time-resolved luminescence measurements showed that the observed luminescence lifetimes of the complexes $[LnL_3]^{3+}$ (Ln^{III} = Nd, Sm, Dy, and Yb) in MeCN at room temperature are in the range of microseconds, with the ytterbium(III) and neodymium(III) compounds having the shortest lifetimes and the samarium(III) and dysprosium(III) complexes the longest (0.6, 51.4, 45.1, and 4.2 μs). The lifetimes and/or luminescence spectra of $[LnL_3]^{3+}$ (Ln^{III} = Pr, Er, and Tm) were too short and/or too weak to be measured with our instrumental setup. However, it is not surprising that $[SmL_3]^{3+}$ and $[DyL_3]^{3+}$ have much shorter luminescence lifetimes than their corresponding compounds with Eu^{III} and Tb^{III} because the Ln^{III} ions with smaller energy gaps (e.g., Dy and Sm) are quenched more efficiently than those with larger energy gaps (e.g., Eu and Tb).[90,92,93] The vibrational deactivation of the luminescent state by OH and/or XH

dx.doi.org/10.1021/ic202094p | *Inorg. Chem.* 2012, 51, 647–660

(X = N or C) oscillators is more efficient when the energy gap between the luminescent- and ground-state manifolds is small. It is also worth noting that the absolute quantum yields of $[LnL_3]^{3+}$ (Ln^{III} = Nd, Sm, Dy, Er, and Yb) determined in MeCN upon ligand excitation are much smaller (1.4×10^{-2}, 2.4×10^{-2}, 1.0×10^{-1}, 3.5×10^{-5}, and 1.9×10^{-3}%; see the Experimental Section) than those of $[EuL_3]^{3+}$ and $[TbL_3]^{3+}$ (1.0 and 8.6%) because their luminescence signal is affected by additional vibrational quenching processes, as was already pointed out during the lifetime discussion. It is worth mentioning that these observations are consistent with other published data.[74,94,95] As stated earlier, the nonradiative deactivation processes are amplified for Ln^{III} ions with small energy gaps and are even more accentuated for NIR-emitting lanthanide(III) complexes.[90,92,93,96] However, the overall weak Ln^{III}-centered NIR luminescence of $[LnL_3]^{3+}$ is also due to the poor efficiency of the energy-transfer processes within the ligand bands (ISC) and between the ligand and the Ln^{III} ions. This is evidenced by the observation of the complexed ligand's emission in the visible region of the luminescence spectra of these systems of interest (Figure 7).

CONCLUSIONS

Contrary to L^8,[58] the optical isomers of **L**, namely, (*R*,*R*)-**1** and (*S*,*S*)-**1**, restored the formation of stable tris complexes in an anhydrous acetonitrile solution, as evidenced by log β_3 values in the range of 23.8. The replacement of the benzyl groups of the carboxamide units in L^8 by phenylethyl substituents revealed that **L** was not locked in a syn,syn,*ZZ* conformation, as seen for L^8. This can be attributed to the steric hindrances resulting from the replacement of one of the two H atoms of the benzyl group in L^8 by a methyl substituent and, consequently, leading to a smaller activation energy barrier for rotation about the OC−N bonds. In addition to the formation of isostructural $[LnL_3]^{3+}$ complexes for the lanthanide(III) series studied (Eu−Yb) in the solid state, the introduction of a chiral asymmetric C atom in each carboxamide moiety led to a diastereomeric resolution of the 9-coordinate lanthanide(III) complexes. Of special importance, the Δ or Λ metal stereochemistry was induced by the chiral nature of the ligand [(*S*,*S*)-**1** or (*R*,*R*)-**1**, respectively].

In addition to these findings supported by the structural and spectroscopic studies performed, it was also shown that the ligand triplet-excited-state energy was relatively well suited to sensitize many Ln^{III} ions emitting in the visible and/or NIR regions. Although the sensitization of these Ln^{III} ions was relatively weak due to poor energy-transfer processes, one can envision using these stable $[LnL_3]^{3+}$ complexes for their chiroptical properties (i.e., large CPL activities observed)[36,38,77] to develop reliable empirical relationships between the chiral structures and CPL sign patterns. Of special importance, one may be able to develop a "helicity rule" aimed at determining a Δ or Λ helicity configuration based upon CPL sign patterns from such Ln^{III}-containing systems or related compounds emitting in the visible and NIR regions. Research in these directions is currently underway.

It is also interesting to note that studies on lanthanide(III) complexes with C_4-symmetrical chiral tetraamide derivative ligands based on 1,4,7,10-tetraazacyclododecane may suggest that there is a correlation between the sign of the torsional angle NCCO or NCCN and the metal stereochemistry.[97,98] It was shown that an *R* configuration at the C center resulted in negative and positive signs for the ring NCCO and C_4-related NCCN torsion angles, associated with Λ and δ configurations, respectively. A similar behavior was found for C_3-symmetric lanthanide(III) complexes of a pyridylphenylphosphinate triazacyclononane based ligand even though this ligand did not exhibit chirality about an amide moiety.[99] In this case, an *R* configuration at the P atom results in positive and negative signs for the ring NCCN and substituent $NCCN_{py}$ torsion angles, associated with an Λ configuration. Although it is premature to conclude that a similar phenomenon applies to D_3-like symmetric lanthanide(III) compounds such as those with **L** and **L′**, one may wonder if, e.g., a negative NCXO or NCCN torsion angle is generally associated with an *R* configuration. However, it is worth pointing out that the same behavior was observed in each of these Ln^{III}-containing systems. That is, Δ or Λ stereochemistry about Ln^{III} was selectively induced by ligand chirality. This potential for a priori selection of the metal stereochemistry will continue to be explored in the forthcoming years.

ASSOCIATED CONTENT

Supporting Information

ES-MS, NMR, and UV/visible spectral data (Figures S1 and S3−S8 and Tables S2 and S11), luminescence sensitization determination, geometric optimization of the three optical isomers of **L** (Figure S2), all X-ray structural data (Figures S9 and S10 and Tables S1 and S3−S11), and CIF including files for all $[LnL_3]^{3+}$ compounds [Ln^{III} = Eu, Gd, Tb, and Yb; **L** = (*R*,*R*)-**1** and (*S*,*S*)-**1**]. This material is available free of charge via the Internet at http://pubs.acs.org.

AUTHOR INFORMATION

Corresponding Author

*E-mail: gilles.muller@sjsu.edu.

ACKNOWLEDGMENTS

The authors thank Dr. Christopher M. Andolina for assistance with lifetime measurements. We also thank Prof. Kenneth N. Raymond of University of California, Berkeley, for the use of his spectrofluorometer, adapted for TCSPC and MCS measurements. Similarly, Prof. Ana de Bettencourt-Dias of University of Nevada, Reno, is thanked for the use of her instrumentation to perform measurements in the NIR region during G.M.'s one-semester visiting position in her research group. G.M. thanks the National Institutes of Health, Minority Biomedical Research Support (1 SC3 GM089589-02 and 3 S06 GM008192-27S1) and the Henry Dreyfus Teacher−Scholar Award for financial support, whereas the NSF (MRI Grant 0923573) is thanked for use of the San José State University Protein Laboratory. E.E.Q. and S.L. thank the NIH (RISE Grant 5R25GM071381) for research fellowships. A.J.I. thanks the Howard Hughes Medical Institute (Award 52006312) for a research fellowship and the 2010 Claudia Greathead Research Stipend at San José State University. A.d.B.D. thanks the University of Nevada, Reno, and the National Science Foundation (Grant CHE 0733458) for financial research support.

REFERENCES

(1) Shinoda, S.; Tsukube, H. *Analyst* **2011**, *136*, 431−435.
(2) Ye, Z.; Chen, J.; Wang, G.; Yuan, J. *Anal. Chem.* **2011**, *83*, 4163−4169.
(3) Fung, Y. O.; Wu, W.; Yeung, C.-T.; Kong, H.-K.; Wong, K. K.-C.; Lo, W.-S.; Law, G.-L.; Wong, K.-L.; Lau, C.-K.; Lee, C.-S.; Wong, W.-T. *Inorg. Chem.* **2011**, *50*, 5517−5525.

(4) Hagan, A. K.; Zuchner, T. *Anal. Bioanal. Chem.* **2011**, *400*, 2847−2864.
(5) Wang, X.; Wang, X.; Wang, Y.; Guo, Z. *Chem. Commun.* **2011**, *47*, 8127−8129.
(6) Liu, X.; Ye, Z.; Wei, W.; Du, Y.; Yuan, J.; Ma, D. *Chem. Commun.* **2011**, *47*, 8139−8141.
(7) Bünzli, J.-C. G. *Chem. Rev.* **2010**, *110*, 2729−2755.
(8) Bünzli, J.-C. G. *Chem. Lett.* **2009**, *38*, 104−109.
(9) Moore, E. G.; Samuel, A. P. .S; Raymond, K. N. *Acc. Chem. Res.* **2009**, *42*, 542−552.
(10) Bünzli, J.-C. G.; Comby, S.; Chauvin, A.-S.; Vandevyver, C. D. B. *J. Rare Earths* **2007**, *25*, 257−274.
(11) Bünzli, J.-C. G. Metal Ions in Biological Systems. In *Metal Complexes in Tumor Diagnosis and as Anticancer Agents*; Sigel, A., Sigel, H., Eds.; Marcel Dekker Inc.: New York, 2004; Vol. *42*, pp 39−75.
(12) Poole, R. A.; Kielar, F.; Richardson, S. L.; Stenson, P. A.; Parker, D. *Chem. Commun.* **2006**, 4084−4086.
(13) Bünzli, J.-C. G. Rare Earth Luminescent Centers in Organic and Biochemical Compounds. In *Spectroscopic Properties of Rare Earths in Optical Materials*; Liu, G., Jacquier, B., Eds.; Springer: Berlin, 2005; Vol. *83*, pp 462−499.
(14) Parker, D.; Yu, J. *Chem. Commun.* **2005**, 3141−3143.
(15) Pal, R.; Parker, D. *Org. Biomol. Chem.* **2008**, *6*, 1020−1033.
(16) Tremblay, M. S.; Lee, M.; Sames, D. *Org. Lett.* **2008**, *10*, 5−8.
(17) Hemmilä, I.; Mukkala, V. M. *Crit. Rev. Clin. Lab. Sci.* **2001**, *38*, 441−519.
(18) Chauvin, A.-S.; Comby, S.; Song, B.; Vandevyver, C. D. B.; Bünzli, J.-C. G. *Chem.—Eur. J.* **2008**, *14*, 1726−1739.
(19) Bünzli, J.-C. G.; Chauvin, A.-S.; Vandevyver, C. D. B.; Bo, S.; Comby, S. *Ann. N.Y. Acad. Sci.* **2008**, *1130*, 97−105.
(20) Chauvin, A.-S.; Comby, S.; Song, B.; Vandevyver, C. D. B.; Thomas, F.; Bünzli, J.-C. G. *Chem.—Eur. J.* **2007**, *13*, 9515−9526.
(21) Law, G.-L.; Wong, K.-L.; Man, C. W.-Y.; Wong, W.-T.; Tsao, S.-W.; Lam, M. H.-W.; Lam, P. K.-S. *J. Am. Chem. Soc.* **2008**, *130*, 3714−3715.
(22) Song, B.; Vandevyver, C. D. B.; Deiters, E.; Chauvin, A.-S.; Hemmilä, I.; Bünzli, J.-C. G. *Analyst* **2008**, *133*, 1749−1756.
(23) Yam, V. W.-W.; Lo, K. K.-W. *Coord. Chem. Rev.* **1998**, *184*, 157−240.
(24) Andraud, C.; Maury, O. *Eur. J. Inorg. Chem.* **2009**, 4357−4371.
(25) Ma, Y.; Wang, Y. *Coord. Chem. Rev.* **2010**, *254*, 972−990.
(26) Muller, G. *Dalton Trans.* **2009**, 9692−9707, (Invited Perspective Article).
(27) Riehl, J. P.; Muller, G. Circularly Polarized Luminescence Spectroscopy and Emission-Detected Circular Dichroism. In *Comprehensive Chiroptical Spectroscopy*; Berova, N., Polavarapu, P. L., Nakanishi, K., Woody, R., Eds.; John Wiley & Sons, Inc., in press.
(28) Riehl, J. P.; Muller, G. Circularly Polarized Luminescence Spectroscopy from Lanthanide Systems. In *Handbook on the Physics and Chemistry of Rare Earths*; Gschneidner, K. A., Jr., Bünzli, J.-C. G., Pecharsky, V. K., Eds.; North-Holland Publishing Co.: Amsterdam, The Netherlands, 2005; Vol. *34*, pp 289−357.
(29) Tsukube, H.; Shinoda, S. *Chem. Rev.* **2002**, *102*, 2389−2403.
(30) Parker, D.; Dickins, R. S.; Puschmann, H.; Crossland, C.; Howard, J. A. K. *Chem. Rev.* **2002**, *102*, 1977−2010.
(31) Brittain, H. G. *J. Coord. Chem.* **1989**, *20*, 331−347.
(32) Brittain, H. G. *Pract. Spectrosc.* **1991**, *12*, 179−200.
(33) Kirschner, S. *J. Indian Chem. Soc.* **1974**, *LI*, 28−31.
(34) Moussa, A.; Pham, C.; Bommireddy, S.; Muller, G. *Chirality* **2009**, *21*, 497−506.
(35) George, M. R.; Golden, C. A.; Grossel, M. C.; Curry, R. J. *Inorg. Chem.* **2006**, *45*, 1739−1744.
(36) Bonsall, S. D.; Houcheime, M.; Straus, D. A.; Muller, G. *Chem. Commun.* **2007**, *35*, 3676−3678.
(37) Muller, G.; Schmidt, B.; Jiricek, J.; Hopfgartner, G.; Riehl, J. P.; Bünzli, J.-C. G.; Piguet, C. *J. Chem. Soc., Dalton Trans.* **2001**, 2655−2662.
(38) Do, K.; Muller, F. C.; Muller, G. *J. Phys. Chem. A* **2008**, *112*, 6789−6793.
(39) Leonard, J. P.; Jensen, P.; McCabe, T.; O'Brien, J. E.; Peacock, R. D.; Kruger, P. E.; Gunnlaugsson, T. *J. Am. Chem. Soc.* **2007**, *129*, 10986−10987.
(40) Yuasa, J.; Ohno, T.; Miyata, K.; Tsumatori, H.; Hasegawa, Y.; Kawai, T. *J. Am. Chem. Soc.* **2011**, *133*, 9892−9902.
(41) *SMART: Area-Detector Package*, version 5.059; Bruker Analytical X-ray Systems, Inc.: Madison, WI, 1999.
(42) *SAINT: SAX Area-Detector Integration Program*, version 7.07B; Siemens Industrial Automation, Inc.: Madison, WI, 2005.
(43) *XPREP: Part of the SHELXTL Crystal Structure Determination Package*, version 6.12; Bruker AXS Inc.: Madison, WI, 1995.
(44) Sheldrick, G. M. *SADABS: Siemens Area Detector Absorption Correction Program*, version 2.10; University of Göttingen: Göttingen, Germany, 2005.
(45) WinGX 1.70.01: Farrugia, L. J. *J. Appl. Crystallogr.* **1999**, *32*, 837−838.
(46) Burla, M. C.; Caliandro, R.; Camalli, M.; Carrozzini, B.; Cascarano, G. L.; De Caro, L.; Giacovazzo, C.; Polidori, G.; Spagna, R. *J. Appl. Crystallogr.* **2005**, *38*, 381−388.
(47) Sheldrick, G. M. *SHELX97, Programs for Crystal Structure Analysis*; Institut für Anorganische Chemie der Universität: Göttingen, Germany, 1998.
(48) Farrugia, L. J. *J. Appl. Crystallogr.* **1997**, *30*, 565.
(49) Spek, A. L. *PLATON—A Multipurpose Crystallographic Tool*; Utrecht University: Utrecht, The Netherlands, 2007.
(50) Demas, J. N.; Crosby, G. A. *J. Phys. Chem.* **1971**, *75*, 991−1024.
(51) Meech, S. R.; Phillips, D. C. *J. Photochem.* **1983**, *23*, 193−217.
(52) Chauvin, A.-S.; Gumy, F.; Imbert, D.; Bünzli, J.-C. G. *Spectrosc. Lett.* **2004**, *37*, 517−532.
(53) Meshkova, S. B.; Topilova, Z. M.; Bolshoy, D. V.; Beltyukova, S. V.; Tsvirko, M. P.; Venchikov, V. Y. *Acta Phys. Pol., A* **1999**, *95*, 983−990.
(54) Brayshaw, P. A.; Bünzli, J.-C. G.; Froidevaux, P.; Harrowfield, J. M.; Kim, Y.; Sobolev, A. N. *Inorg. Chem.* **1995**, *34*, 2068−2076.
(55) Charles, R. G.; Ohlmann, R. C. *J. Inorg. Nucl. Chem.* **1965**, *27*, 255−259.
(56) Gans, P.; Sabatini, A.; Vacca, A. *Talanta* **1996**, *43*, 1739−1753.
(57) Shao, Y.; Molnar, L. F.; Jung, Y.; Kussmann, J.; Ochsenfeld, C.; Brown, S. T.; Gilbert, A. T. B.; Slipchenko, L. V.; Levchenko, S. V.; O'Neill, D. P.; DiStasio, R. A. Jr.; Lochan, R. C.; Wang, T.; Beran, G. J. O.; Besley, N. A.; Herbert, J. M.; Lin, C. Y.; Van Voorhis, T.; Chien, S. H.; Sodt, A.; Steele, R. P.; Rassolov, V. A.; Maslen, P. E.; Korambath, P. P.; Adamson, R. D.; Austin, B.; Baker, J.; Byrd, E. F. C.; Dachsel, H.; Doerksen, R. J.; Dreuw, A.; Dunietz, B. D.; Dutoi, A. D.; Furlani, T. R.; Gwaltney, S. R.; Heyden, A.; Hirata, S.; Hsu, C.-P.; Kedziora, G.; Khalliulin, R. Z.; Klunzinger, P.; Lee, A. M.; Lee, M. S.; Liang, W.; Lotan, I.; Nair, N.; Peters, B.; Proynov, E. I.; Pieniazek, P. A.; Rhee, Y. M.; Ritchie, J.; Rosta, E.; Sherrill, C. D.; Simmonett, A. C.; Subotnik, J. E.; Woodcock, H. L., III; Zhang, W.; Bell, A. T.; Chakraborty, A. K.; Chipman, D. M.; Keil, F. J.; Warshel, A.; Hehre, W. J.; Schafer, H. L., III; Kong, J.; Krylov, A. I.; Gill, P. M. W.; Head-Gordon, M. *Phys. Chem. Chem. Phys.* **2006**, *8*, 3172−3191.
(58) Le Borgne, T.; Bénech, J.-M.; Floquet, S.; Bernardinelli, G.; Aliprandini, C.; Bettens, P.; Piguet, C. *Dalton Trans.* **2003**, 3856−3868.
(59) Malone, J. F.; Murray, C. M.; Dolan, G. M. *Chem. Mater.* **1997**, *9*, 2983−2989.
(60) Meghdadi, S.; Nalchigar, S.; Khavasi, H. R. *Acta Crystallogr.* **2008**, *E64*, o431.
(61) Becke, A. D. *J. Chem. Phys.* **1993**, *98*, 1372−1377.
(62) Becke, A. D. *J. Chem. Phys.* **1993**, *98*, 5648−5652.
(63) Petersson, G. A.; Bennett, A.; Tensfeldt, T. G.; Al-Laham, M. A.; Shirley, W. A.; Mantzaris, J. *J. Chem. Phys.* **1988**, *89*, 2193−2218.
(64) Petersson, G. A.; Al-Laham, M. A. *J. Chem. Phys.* **1991**, *94*, 6081−6090.
(65) Muller, G.; Riehl, J. P.; Schenk, K. J.; Hopfgartner, G.; Piguet, C.; Bünzli, J.-C. G. *Eur. J. Inorg. Chem.* **2002**, 3101−3110.

(66) Muller, G.; Bünzli, J.-C. G.; Schenk, K. J.; Piguet, C.; Hopfgartner, G. *Inorg. Chem.* **2001**, *40*, 2642−2651.
(67) Renaud, F.; Piguet, C.; Bernardinelli, G.; Bünzli, J.-C. G.; Hopfgartner, G. *Chem.—Eur. J.* **1997**, *3*, 1660−1667.
(68) Renaud, F.; Piguet, C.; Bernardinelli, G.; Bünzli, J.-C. G.; Hopfgartner, G. *Chem.—Eur. J.* **1997**, *3*, 1646−1659.
(69) Muller, G.; Maupin, C. L.; Riehl, J. P.; Birkedal, H.; Piguet, C.; Bünzli, J.-C. G. *Eur. J. Inorg. Chem.* **2003**, 4065−4072.
(70) Muller, G.; Bünzli, J.-C. G.; Riehl, J. P.; Suhr, D.; von Zelewsky, A.; Mürner, H. *Chem. Commun.* **2002**, 1522−1523.
(71) Seitz, M.; Moore, E. G.; Ingram, A. J.; Muller, G.; Raymond, K. N. *J. Am. Chem. Soc.* **2007**, *129*, 15468−15470.
(72) Samuel, A. P. S.; Lunkley, J. L.; Muller, G.; Raymond, K. N. *Eur. J. Inorg. Chem.* **2010**, 3343−3347.
(73) Seitz, M.; Do, K.; Ingram, A. J.; Moore, E. G.; Muller, G.; Raymond, K. N. *Inorg. Chem.* **2009**, *48*, 8469−8479.
(74) D'Aléo, A.; Xu, J.; Do, K.; Muller, G.; Raymond, K. N. *Helv. Chim. Acta* **2009**, *92*, 2439−2460.
(75) Shannon, R. D. *Acta Crystallogr.* **1976**, *A32*, 751−767.
(76) Tanase, S.; Gallego, P. M.; de Gelder, R.; Fu, W. T. *Inorg. Chim. Acta* **2007**, *360*, 102−108.
(77) Hua, K. T.; Lopez, S.; Ponce, S. G., Jr.; Muller, G., manuscript in preparation.
(78) Steemers, F. J.; Verboom, W.; Reinhoudt, D. N.; van der Tol, E. B.; Verhoeven, J. W. *J. Am. Chem. Soc.* **1995**, *117*, 9408−9414.
(79) Tobita, S. *J. Phys. Chem.* **1985**, *89*, 5649−5654.
(80) Tobita, S.; Arakawa, M.; Tanaka, I. *J. Phys. Chem.* **1984**, *88*, 2697−2702.
(81) Parker, D. *Coord. Chem. Rev.* **2000**, *205*, 109−130.
(82) Parker, D.; Williams, J. A. G. *J. Chem. Soc., Dalton Trans.* **1996**, 3613−3628.
(83) Senegas, J.-M.; Bernardinelli, G.; Imbert, D.; Bünzli, J.-C. G.; Morgantini, P.-Y.; Weber, J.; Piguet, C. *Inorg. Chem.* **2003**, *42*, 4680−4695.
(84) Quici, S.; Cavazzini, M.; Marzanni, G.; Accorsi, G.; Armaroli, N.; Ventura, B.; Barigelletti, F. *Inorg. Chem.* **2005**, *44*, 529−537.
(85) Chen, X.-Y.; Yang, X.; Holliday, B. J. *Inorg. Chem.* **2010**, *49*, 2583−2585.
(86) Mato-Iglesias, M.; Rodríguez-Bias, T.; Platas-Iglesias, C.; Starck, M.; Kadjane, P.; Ziessel, R.; Charbonnière, L. *Inorg. Chem.* **2009**, *48*, 1507−1518.
(87) Kang, T.-S.; Harrison, B. S.; Bouguettaya, M.; Foley, T. J.; Boncella, J. M.; Schanze, K. S.; Reynolds, J. R. *Adv. Funct. Mater.* **2003**, *13*, 205−210.
(88) Gonçalves e Silva, F. R.; Malta, O. L.; Reinhard, C.; Güdel, H.-U.; Piguet, C.; Moser, J. E.; Bünzli, J. C. G. *J. Phys. Chem. A* **2002**, *106*, 1670−1677.
(89) Moore, E. G.; Szigethy, G.; Xu, J.; Pålsson, L.-O.; Beeby, A.; Raymond, K. N. *Angew. Chem., Int. Ed.* **2008**, *47*, 9500−9503.
(90) Davies, G. M.; Aarons, R. J.; Motson, G. R.; Jeffrey, J. C.; Adams, H.; Faulkner, S.; Ward, M. D. *Dalton Trans.* **2004**, 1136−1144.
(91) Dang, S.; Yu, J.; Wang, X.; Sun, L.; Deng, R.; Feng, J.; Fan, W.; Zhang, H. *J. Lumin.* **2011**, *131*, 1857−1863.
(92) Haas, Y.; Stein, G.; Würzberg, E. *J. Chem. Phys.* **1974**, *60*, 258−263.
(93) Wolbers, M. P. O.; van Veggel, F. C. J. M.; Snellink-Ruël, B. H. M.; Hofstraat, J. W.; Geurts, F. A. J.; Reinhoudt, D. N. *J. Chem. Soc., Perkin Trans. 2* **1998**, 2141−2150.
(94) Lewis, D. J.; Glover, P. B.; Solomons, M. C.; Pikramenou, Z. *J. Am. Chem. Soc.* **2011**, *133*, 1033−1043.
(95) Petoud, S.; Muller, G.; Moore, E. G.; Xu, J.; Sokolnicki, J.; Riehl, J. P.; Le, U. N.; Cohen, S. M.; Raymond, K. N. *J. Am. Chem. Soc.* **2007**, *129*, 77−83.
(96) Hebbink, G. A.; Reinhoudt, D. N.; van Veggel, F. C. J. M. *Eur. J. Org. Chem.* **2001**, *21*, 4101−4106.
(97) Dickins, R. S.; Howard, J. A. K.; Maupin, C. L.; Moloney, J. M.; Parker, D.; Riehl, J. P.; Siligardi, G.; Williams, J. A. G. *Chem.—Eur. J.* **1999**, *5*, 1095−1105.
(98) Dickins, R. S.; Howard, J. A. K.; Moloney, J. M.; Parker, D.; Peacock, R. D.; Siligardi, G. *Chem. Commun.* **1997**, 1747−1748.
(99) Walton, J. W.; Di Bari, L.; Parker, D.; Pescitelli, G.; Puschmann, H.; Yufit, D. S. *Chem. Commun.* **2011**, *47*, 12289−12291.